Title

tRNA Genes Affect Chromosome Structure and Function via Local Effects.

Journal

Molecular and Cellular Biology, 39(8)

Authors

Hamdani, Omar

Dhillon, Namrita

Hsieh, Tsung-Han

et al.

Publication Date

2019-04-15

DOI

10.1128/MCB.00432-18

AMERICAN SOCIETY FOR MICROBIOLOGY | Molecular and Cellular Biology®

RESEARCH ARTICLE

tRNA Genes Affect Chromosome Structure and Function via Local Effects

Omar Hamdani,[a] Namrita Dhillon,[a] Tsung-Han S. Hsieh,[b] Takahiro Fujita,[c] Josefina Ocampo,[d] Jacob G. Kirkland,[a] Josh Lawrimore,[e] Tetsuya J. Kobayashi,[f] Brandon Friedman,[e] Derek Fulton,[e] Kenneth Y. Wu,[a] Răzvan V. Chereji,[d] Masaya Oki,[c] Kerry Bloom,[e] David J. Clark,[d] Oliver J. Rando,[b] Rohinton T. Kamakaka[a]

[a]Department of MCD Biology, University of California, Santa Cruz, California, USA
[b]Department of Biochemistry and Molecular Pharmacology, University of Massachusetts Medical School, Worcester, Massachusetts, USA
[c]Department of Applied Chemistry Biotechnology, University of Fukui, Fukui, Japan
[d]Division of Developmental Biology, Eunice Kennedy Shriver National Institute of Child Health and Human Development, Bethesda, Maryland, USA
[e]Department of Biology, University of North Carolina at Chapel Hill, Chapel Hill, North Carolina, USA
[f]Institute of Industrial Science, The University of Tokyo, Tokyo, Japan

ABSTRACT The genome is packaged and organized in an ordered, nonrandom manner, and specific chromatin segments contact nuclear substructures to mediate this organization. tRNA genes (tDNAs) are binding sites for transcription factors and architectural proteins and are thought to play an important role in the organization of the genome. In this study, we investigate the roles of tDNAs in genomic organization and chromosome function by editing a chromosome so that it lacked any tDNAs. Surprisingly our analyses of this tDNA-less chromosome show that loss of tDNAs does not grossly affect chromatin architecture or chromosome tethering and mobility. However, loss of tDNAs affects local nucleosome positioning and the binding of SMC proteins at these loci. The absence of tDNAs also leads to changes in centromere clustering and a reduction in the frequency of long-range *HML-HMR* heterochromatin clustering with concomitant effects on gene silencing. We propose that the tDNAs primarily affect local chromatin structure, which results in effects on long-range chromosome architecture.

KEYWORDS chromatin, nucleosome, SMC proteins, *Saccharomyces cerevisiae*, chromosome structure, gene silencing, tDNA

The three-dimensional (3D) organization of the *Saccharomyces cerevisiae* nucleus is nonrandom (reviewed in references 1 and 2). Each chromosome occupies a specific territory in the nucleus anchored to nuclear substructures via specific DNA sequences. The telomeres of each chromosome tend to associate with one another and with the nuclear envelope in small clusters, based on the lengths of the chromosome arms (3–5). The ribosomal DNA (rDNA) repeats on chromosome XII are packaged into a dense structure known as the nucleolus, which also localizes to the nuclear periphery (6). Opposite the nucleolus is the spindle pole body, which is the interphase attachment site for the centromeres (CEN) of the 16 chromosomes (7). Attachment of centromeres to the spindle pole and attachment of telomeres to the nuclear membrane depending upon chromosome arm length help organize the nucleus (8). The active genes along the chromosome arms primarily reside in the nuclear interior, though some active genes, including some tRNA genes, interact with nuclear pores and help tether the arms (1, 9, 10).

Besides DNA sequence elements, numerous proteins play a role in nuclear organization via networks of interactions between nuclear-membrane and chromatin-bound proteins. Chromatin-bound proteins involved in this organization include heterochro-

Citation Hamdani O, Dhillon N, Hsieh T-HS, Fujita T, Ocampo J, Kirkland JG, Lawrimore J, Kobayashi TJ, Friedman B, Fulton D, Wu KY, Chereji RV, Oki M, Bloom K, Clark DJ, Rando OJ, Kamakaka RT. 2019. tRNA genes affect chromosome structure and function via local effects. Mol Cell Biol 39:e00432-18. https://doi.org/10.1128/MCB.00432-18.

Address correspondence to Rohinton T. Kamakaka, rohinton@ucsc.edu.

O.H., N.D., T-H.S.H., T.F., and J.O. contributed equally to this work.

Received 6 September 2018
Returned for modification 1 October 2018
Accepted 18 January 2019
Accepted manuscript posted online 4 February 2019
Published 2 April 2019

matin proteins (11), lamin-like proteins (12–16), specific transcription factors (17, 18), RNA polymerases (6), and DNA repair proteins (19, 20; reviewed in reference 1).

tRNA genes (tDNAs) are a class of active genes found on all chromosomes and are bound by transcription factors TFIIIB and TFIIIC and RNA polymerase (Pol) III. tDNAs are short, highly transcribed DNA sequences (21) that are usually nucleosome free with strongly positioned flanking nucleosomes (22–25). The tDNAs contain internal promoter elements called A and B boxes, which aid in the binding of the transcription factor TFIIIC (26, 27). TFIIIC helps recruit TFIIIB to AT-rich sequences upstream of the tDNA. tDNA-bound transcription factors function via interactions with cofactors. tRNA genes are sites of binding for numerous chromatin proteins, including the architectural SMC proteins, nuclear pore proteins, chromatin remodelers, and histone modifiers. Studies from several laboratories have shown that tDNAs are enriched in cohesin (Smc1/Smc3) (28) and condensin (Smc2/Smc4) complexes (29, 30), as well as the SMC-loading proteins (Scc2/Scc4) (31, 32) and some chromatin remodelers, including RSC (22, 29, 33–35).

While individual tRNA genes turn over rapidly as a result of mutational inactivation and gene loss (36–38), a subset of tDNAs are syntenic with respect to neighboring sequences (39, 40), and data suggest that these conserved tDNAs possess chromosome position-specific functions in gene regulation (reviewed in references 41 and 42). There are several position-specific effects mediated by tDNAs. First, tDNAs have been shown to function as heterochromatin barrier insulators, which stop the spread of heterochromatic domains into adjacent nonsilenced domains (35, 39, 43, 44). Second, tDNAs block communication between enhancers and promoters when located between these elements in yeast, *Drosophila*, mouse, and human cells by acting as enhancer blockers (39, 45–50). Third, the presence of a tDNA in close proximity to an RNA Pol II-transcribed gene promoter antagonizes transcription from the Pol II-transcribed gene in a phenomenon referred to as tRNA gene-mediated (tgm) silencing (30, 51, 52).

In many organisms, tDNAs have also been shown to cluster at sites in the nucleus (39, 42, 53–55). In *S. cerevisiae*, DNA fluorescent *in situ* hybridization (FISH) studies have shown that some tDNAs cluster together adjacent to centromeres (52, 54), while proximity ligation analysis suggests that tDNAs cluster at the outer periphery of the nucleolus, as well as near the centromeres (10), though more recent genome-wide chromosome conformation capture (HiC) studies seem unable to detect these long-range associations (56). Based on these results, it has been proposed that TFIIIC binding to discrete sites along the chromosome plays an important role in chromosome folding and organization in the yeast nucleus (54, 57, 58).

To better analyze the role of tDNAs in chromatin looping and organization, we generated a "tDNA-less" chromosome through the systematic deletion of all the tDNAs on chromosome III in *S. cerevisiae*. We characterized the chromatin packaging, chromosome folding, and nuclear dynamics of this chromosome. We show that tDNA loss affects nucleosome positioning and loading of SMC proteins in the vicinity of tDNAs but that this has no effect on chromatin looping. While loss of the tDNAs does not affect chromatin looping, it does affect centromere clustering and the long-range interactions of the silenced *HML* and *HMR* loci with concomitant effects on gene silencing.

RESULTS

The ~275 tDNAs in the budding yeast genome are dispersed across all 16 chromosomes. Here, we focus on chromosome III, which is 316 kb long and has two tDNAs on the left arm and eight tDNAs on the right arm. In order to investigate the roles of tDNAs in chromatin looping and nuclear organization and function, we created a strain in which chromosome III is devoid of any functional tDNAs by deleting an internal fragment of each tDNA. The deletions eliminate the internal promoter elements (both BoxA and BoxB) and thus eliminate the binding of the transcription factors TFIIIC and TFIIIB. For simplicity, we have labeled the tDNA adjacent to the *HMR* locus t0 and have labeled the remaining nine tDNAs, from right to left, t1, t2, t3, etc. To delete the tDNAs, we first replaced an internal segment of the gene with a *URA3* gene and then

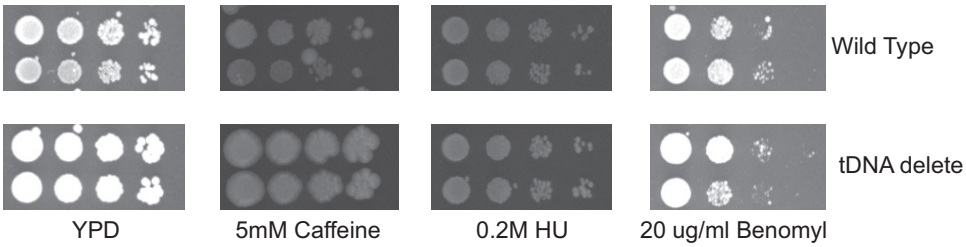

FIG 1 Drug sensitivity of wild-type and tDNA delete strains. Tenfold serial dilutions of cells starting at 10^7 cells were spotted on YPD plates with different concentrations of various drugs and allowed to grow for between 2 and 5 days. HU, hydroxyurea.

subsequently replaced *URA3* with a DNA fragment containing a unique DNA bar code. This involved multiple sequential transformations. Each deletion was monitored by PCR analysis, and intermediate strains were backcrossed to the wild-type (WT) strain W-303 prior to additional rounds of transformations. All of the experiments described were performed in this strain background to avoid strain-specific effects.

Most tRNA isoacceptor families have multiple copies scattered throughout the genome, though single gene copies code for six isoacceptor families. On chromosome III, 8 of the 10 tDNAs that were deleted are members of multicopy gene families (with 10 to 16 copies in the genome) and are not essential. However, tDNA t1 [*tS*(*CGA*)*C*] is a single-copy gene and is essential in *S. cerevisiae* (59), and there are only two copies of tDNA t7 [*tP*(*AGG*)*C*] in the genome. Loss of t7 from chromosome III caused cells to grow more slowly. In order to remove these two genes from chromosome III and simultaneously maintain the health of the yeast, we integrated single copies of the two genes on chromosome XV at the *HIS3* locus. Once the full tDNA deletion chromosome III had been constructed, the strain harboring the chromosome was backcrossed with wild-type W-303, and segregation of the deleted tDNAs was monitored by PCR using primers specific to the unique bar codes. The sequence of this modified chromosome is available.

The strain in which chromosome III lacked any tDNAs (tDNA delete) was grown in rich medium at 30°C and did not show any obvious growth defect, forming homogeneous and healthy, smooth-edged colonies. Strains bearing this tDNA-less chromosome had a doubling time of ~90 min in liquid yeast extract-peptone-dextrose (YPD) medium, which was indistinguishable from a wild-type strain. This is consistent with data showing that loss of one copy of multicopy tDNAs in yeast cells does not lead to growth defects in rich medium (60).

We analyzed the wild-type and tDNA mutant strains for sensitivity to various stresses. We grew haploid cells on plates containing increasing concentrations of hydroxyurea, benomyl, and caffeine. This analysis showed that the tDNA delete strain was as resistant to these drugs as the wild-type cells (Fig. 1).

Changes to the local nucleosome landscape surrounding tDNAs. The stable binding of TFIIIC and TFIIIB, as well as their interactions with chromatin remodelers, results in nucleosome eviction at the tDNA and positioning of nucleosomes adjacent to the gene (22, 61). At some tRNA genes, a single nucleosome appears to be disrupted, while at other tDNAs, multiple nucleosomes are disrupted. Since tDNAs are dispersed across the chromosome and are highly transcribed, we first asked if loss of all 10 tDNAs from the chromosome altered the nucleosome and transcription landscape of the chromosome. In order to determine if tDNAs affect nucleosome positions across chromosome III, we mapped nucleosomes in our tDNA delete strain, as well as in the wild-type strain.

Haploid yeast cells were grown to log phase and harvested, and nuclei were digested with various concentrations of micrococcal nuclease (MNase) to generate mononucleosome-protected DNAs, which were subjected to paired-end MNase-assisted sequencing (MNase-seq). Overall, the nucleosome landscape across all chro-

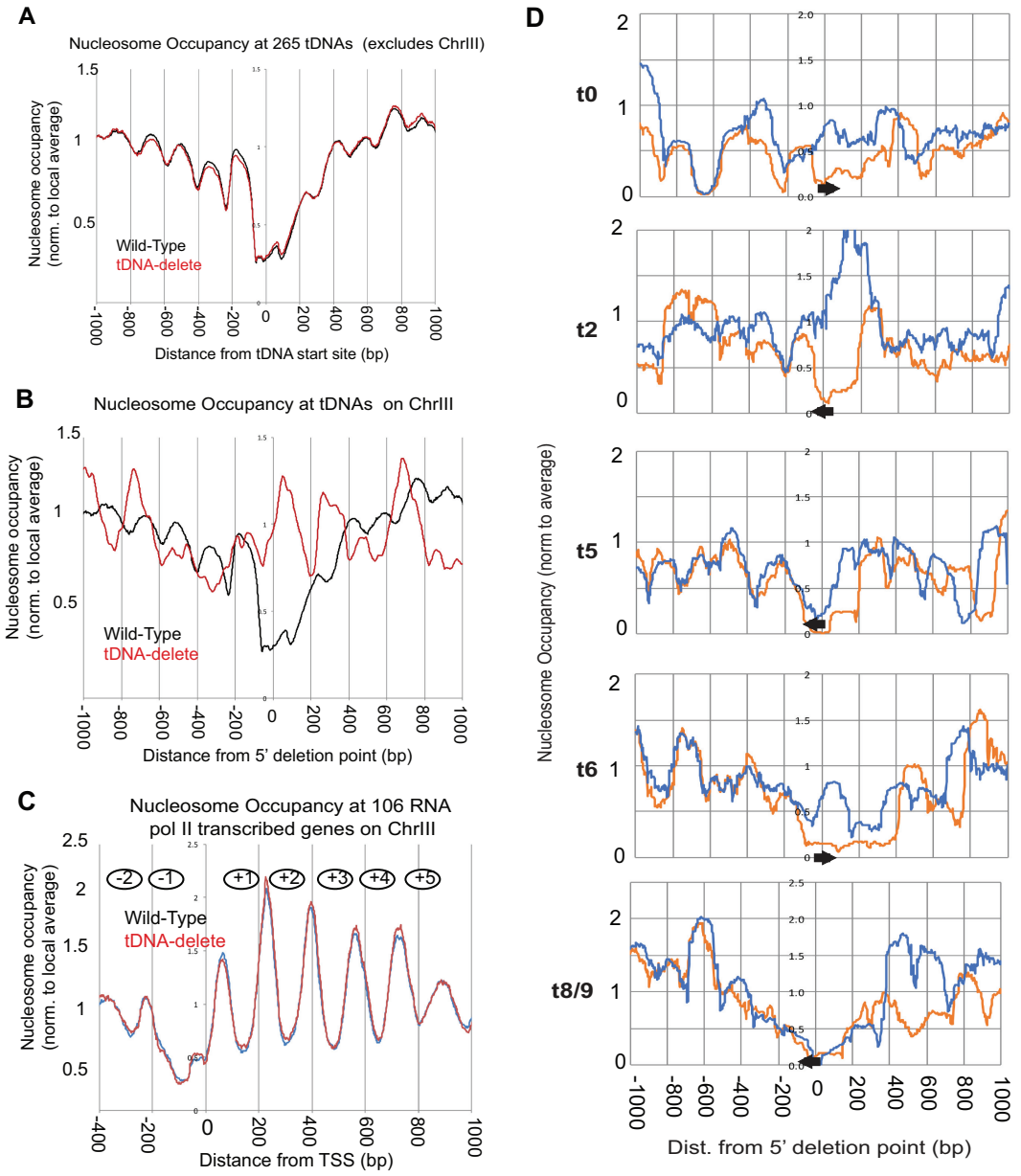

FIG 2 Deletion of tDNAs leads to local changes in chromatin structure. (A) Comparison of nucleosome occupancy rates at 265 tDNAs on all of the yeast chromosomes except chromosome III (ChrIII). The tDNAs were aligned with respect to their transcription start sites (TSS) (set at 0). (B) Analysis of the nucleosome occupancy at tDNAs on chromosome III in the wild-type and tDNA delete strains. (C) Comparison of global nucleosome phasing on chromosome III in wild-type and tDNA delete cells. Shown are the average nucleosome dyad positions on 106 RNA Pol II-transcribed genes on chromosome III. These genes cover most of chromosome III. The genes were aligned with respect to their TSS (set at 0). The average nucleosome dyad density was set at 1. (D) MNase-seq data for wild-type and tDNA delete strains (normalized to the genomic average [i.e., 1]). Coverage plots are shown using all DNA fragments in the 120- to 180-bp range. The reference point (0) is the nucleotide marking the 5′ end of the deletion on chromosome III. Upstream of the deletion point at 0, the DNA sequence is the same in wild-type and the tDNA delete chromosomes III. Downstream of the deletion point, the DNA sequences are different. The arrows show the locations and orientations of the tDNAs in wild-type chromosome III. Meaningful plots could not be made for two tDNAs [*tP*(*AGG*)*C* and *tS*(*CGA*)*C*] because they were moved to another chromosome. Two other tDNAs [*tM*(*CAU*)*C* and *tK*(*CUU*)*C*] are present in S288C strains but are naturally absent in W-303 strains, including the strains used here. Orange, wild-type profile; blue, tDNA delete profile.

mosomes except chromosome III was unaffected by the presence or absence of the chromosome III tDNAs. More focused analysis showed no change in nucleosome positioning in the proximity of the 265 tDNAs scattered on the 15 chromosomes that were not manipulated in this study (Fig. 2A).

In contrast, changes in nucleosome occupancy were observed at or immediately adjacent to the deleted tDNAs on chromosome III. Figure 2B shows the average nucleosome occupancy across 2-kb segments centered on the chromosome III tDNAs, with each tDNA in WT cells aligned at its 5′ end, while in the tDNA delete strain, the 5′ ends of the deletion points were aligned. In the wild-type strain, there is a clear nucleosome-free region centered on the tDNA flanked by positioned nucleosomes reflecting differential digestion of the TFIIIB-TFIIIC complex relative to nucleosomes (35, 62). In the tDNA delete strain, this pattern is altered, and a nucleosome is usually formed over the deletion junction (Fig. 2D). We were unable to determine the change in the chromatin landscape around t1 and t7 tDNAs, since these two genes with 100 bp of flanking sequence were transposed to the *HIS3* locus. Nucleosome positions elsewhere on chromosome III that were distant from the tDNAs were not altered on the tDNA-less chromosome (Fig. 2C). These results demonstrate that tDNAs create nucleosome-free regions at the tRNA gene with positioned nucleosomes flanking the gene. The data also show that their chromatin-organizing effects are locally confined and do not extend beyond their immediate vicinity.

tDNA loss affects expression of few RNA Pol II-transcribed genes. The presence of a tDNA in close proximity to an RNA Pol II-transcribed gene promoter antagonizes transcription from the Pol II-transcribed gene, called tRNA gene-mediated silencing (tgm silencing) (30, 51, 52). In addition, tDNAs have also been shown to function as enhancer blockers when located between an upstream activation sequence (UAS) enhancer and a promoter (47). Since the loss of the tDNAs altered nucleosomes in their vicinity, we wondered if these alterations affected the transcription landscape of genes on chromosome III. Rather than restrict the analysis to Pol II-transcribed genes adjacent to the tDNAs on chromosome III, we investigated the effects of tDNA loss on all Pol II-transcribed genes in the genome and analyzed the changes in RNA levels in the wild type and the tDNA delete strain by transcriptome sequencing (RNA-seq). Total RNA was extracted from exponentially growing yeast cultures, and RNA-seq libraries were prepared, sequenced, and analyzed as described in Materials and Methods. The RNA levels of a very small number of genes were affected upon deletion of the tDNAs. Table 1 lists the genes that were either upregulated or downregulated in the strain lacking tDNAs on chromosome III. Of the 10 tDNAs present on chromosome III, tDNAs t0, t8, and t9 were flanked by retrotransposon elements, and since these are repetitive elements, the tDNA-mediated transcription effects could not be investigated for the loci. Furthermore, tDNAs t3 and t4 are missing in W-303. The expression of only two genes on chromosome III was affected, and in both instances, a tDNA (t1 or t6) was located adjacent to the gene. In one instance, the gene was upregulated upon tDNA loss, while in the second instance, the gene was downregulated. Furthermore, we observed the upregulation of the *MRM1* gene. This gene resides immediately adjacent to *HIS3*. The tDNAs for t1 and t7 were ectopically inserted at the *HIS3* locus in the tDNA delete strain, demonstrating that the ectopic insertion of the tDNAs was the cause of the change in expression of *MRM1*. These data suggest that tDNA-mediated position effects are highly context dependent and affect only some Pol II-transcribed genes and not others.

Of the genes that were downregulated in the tDNA delete strain, several are involved in amino acid biosynthesis, though these genes are scattered throughout the genome and do not localize near tDNAs. The reason expression of these genes was reduced is unclear, given that the two yeast strains used are isogenic with respect to nutritional markers and there are between 10 and 16 copies of each of the six deleted tDNAs in the genome (t0, 11 copies; t2, 10 copies; t5, 16 copies; t6, 11 copies; t8, 10 copies; and t9, 15 copies). It is possible that there is a reduction in transcript levels of these genes due to the small reduction in the tDNA copy number without any other cell phenotype. This is consistent with a recent study where single tDNAs in yeast were deleted, and these single deletions in multicopy tDNA families also led to changes in the expression of a small set of genes involved in translation (60).

Scc2 binding at tDNAs is dependent upon a functional tDNA, but other binding sites are tDNA independent. The SMC proteins play an important role in nuclear

TABLE 1 Genes whose mRNA levels changed in the tDNA delete strain compared to the wild type and statistical analysis of the differences in expression levels

Gene	*Q* value		Beta statistic	Gene product function
	Likelihood ratio test	Wald test		
Upregulated				
YCR061w	0.042003857	3.22E−11	0.6580998	Protein of unknown function
YDL124w	0.042003857	6.31E−14	0.4395261	NADPH-dependent alpha-keto amide reductase
YHR214c-B	0.005672182	2.35E−210	2.5870238	Retrotransposon TYA Gag and TYB Pol genes
YNL160w	0.040272092	2.69E−20	0.5348964 YGP1	Cell wall-related secretory glycoprotein
YOR201c	0.020396347	9.18E−27	0.7685378 MRM1	Ribose methyltransferase
YOR202w	0.009117145	1.20E−76	3.7326308 HIS3	Imidazoleglycerol-phosphate dehydratase
YPL240c	0.042003857	1.20E−15	0.5188043 HSP82	Hsp90 chaperone
Downregulated				
YBR068c	0.030966243	1.53E−20	−0.5156825 BAP2	High-affinity leucine permease
YBR296c	0.039894621	1.87E−19	−0.5692597 PHO89	Plasma membrane Na^+/P_i cotransporter
YCR008w	0.015662463	6.48E−43	−1.1217 SAT4	Ser/Thr protein kinase involved in salt tolerance
YER073w	0.045197971	8.81E−16	−0.5691673 ALD5	Mitochondrial aldehyde dehydrogenase
YER091c	0.042003857	1.79E−20	−0.5345605 MET6	Cobalamin-independent methionine synthase
YGL009c	0.009117145	1.47E−82	−2.0202761 LEU1	Isopropylmalate isomerase
YHR208w	0.007776891	7.72E−106	−1.3235331 BAT1	Mitochondrial branched-chain amino acid aminotransferase
YJR010w	0.042003857	3.34E−13	−0.8073784 MET3	ATP sulfurylase involved in methionine metabolism
YJR016c	0.017736878	3.09E−29	−0.5823368 ILV3	Dihydroxy acid dehydratase involved in biosynthesis of branched-chain amino acids
YKL030w	0.042003857	3.46E−11	−0.6718075	Dubious open reading frame
YKL120w	0.007776891	1.47E−94	−1.4546702 OAC1	Mitochondrial inner membrane transporter
YLR355c	0.042003857	2.35E−12	−0.387429 ILV5	Acetohydroxy acid reductoisomerase involved in biosynthesis of branched-chain amino acids
YMR108w	0.042003857	3.72E−15	−0.4213145 ILV2	Acetolactate synthase involved in isoleucine and valine biosynthesis
YOR271c	0.027535084	4.63E−26	−0.5903308 FSF1	Putative protein of the sideroblastic-associated protein family

organization (63), and tDNAs are major binding sites for SMC proteins and the SMC loaders Scc2/Scc4 and Rsc. Our nucleosome-mapping data indicated that loss of the tDNAs altered nucleosome positions at tDNAs. Since nucleosome-free tDNAs are sites for the recruitment of RSC and Scc2/Scc4 proteins (31, 34, 64, 65), we asked if loss of all the tDNAs on chromosome III reduced recruitment of Scc2 proteins at these loci and whether it also affected loading of Scc2 at other sites along the chromosome.

We performed chromatin immunoprecipitation sequencing (ChIP-seq) of Myc-tagged Scc2 to compare the distributions of the protein genome-wide in the WT and tDNA delete strains (Fig. 3). This analysis showed Scc2 binding at multiple sites along the chromosome, including tDNAs. At some tDNAs, the Scc2 binding was focused, forming a sharp peak, while at other tDNAs, the binding was spread over a wider region. Comparison between the wild type and the tDNA delete strain showed that Scc2 levels did not decrease at any of the sites on the 15 chromosomes. Upon tDNA loss, Scc2 binding decreased at the tDNA loci on chromosome III or at sites in the immediate vicinity of tDNAs, such as *LEU2* (adjacent to tDNA t8) (Fig. 3) and *HMR* (adjacent to t0). On chromosome III, the analysis also showed that there was no significant change in Scc2 binding at other non-tDNA sites on the chromosome. For example, we saw a large peak of Scc2 binding at Tel3L. This peak at Tel3L was unchanged upon tDNA deletion, and similarly, we did not record any change in Scc2 levels at centromere III (*CEN3*), confirming that tDNAs are not the sole determinants for the recruitment of Scc2 to chromosomes.

We confirmed this result by ChIP-quantitative PCR (qPCR) against Scc2. A site at the *OCA4* gene was used as an internal control, since the site does not bind Scc2 in wild-type cells. We were unable to design unique primers at t6 due to the presence of repetitive sequences in the immediate vicinity of the gene and therefore could not map the localization of these proteins at the tDNA. Some primer pairs flank the tDNAs, while others are adjacent to the tDNAs. Consistent with the ChIP-seq data, in wild-type cells, Scc2 was enriched at several of the tDNAs present on chromosome III (Fig. 4A). We observed ~3.5-fold enrichment at t8 and ~2.5-fold enrichment at t0, t2, and t5. When

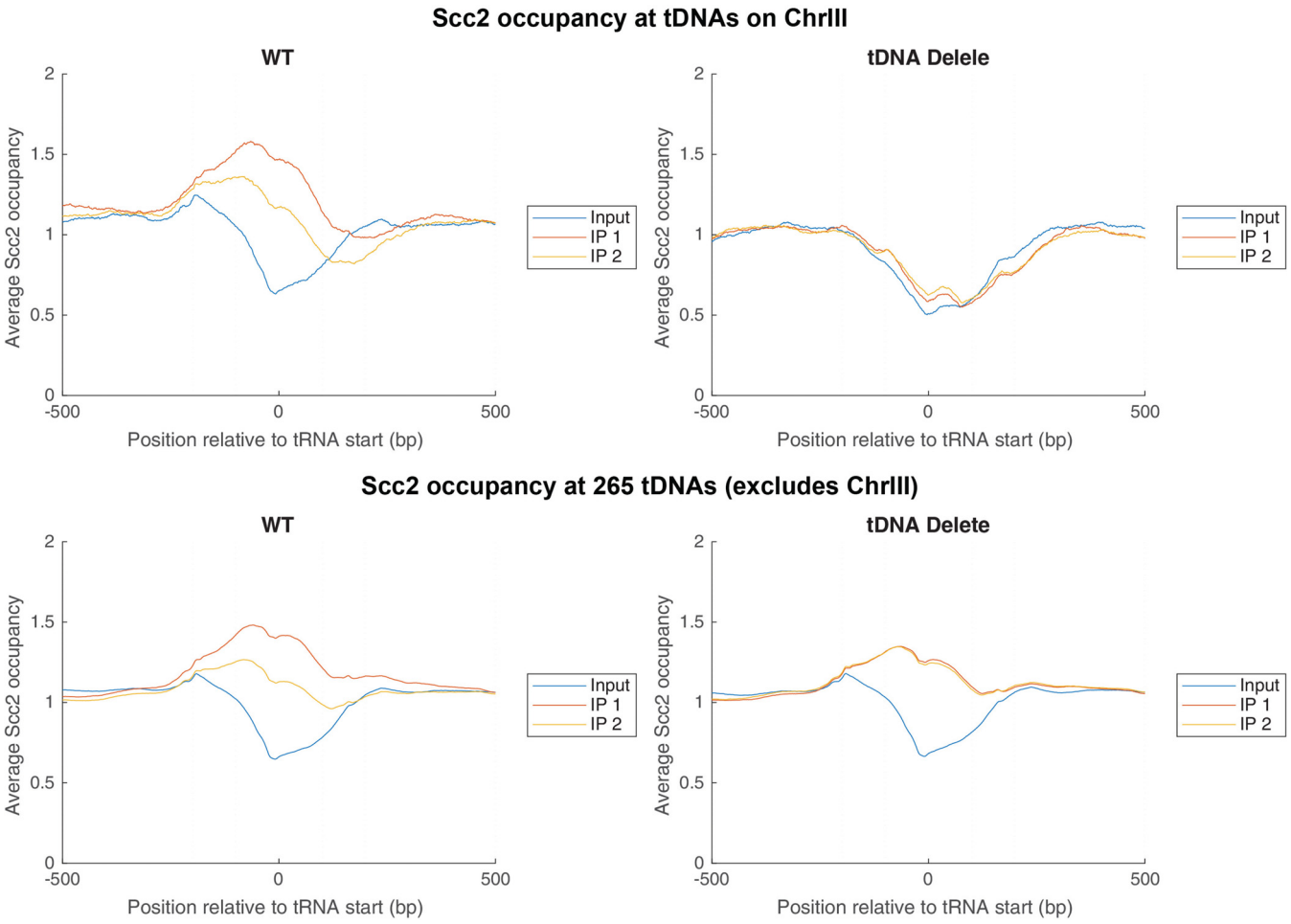

FIG 3 Scc2 binding along chromosome III in the wild-type and tDNA delete strains. Shown is ChIP-seq mapping of Myc-Scc2. (Top) Distribution of Scc2 at tDNAs on chromosome III in wild-type cells (left) and tDNA delete strains (right). (Bottom) Distribution of Scc2 at 265 tDNAs on all chromosomes except chromosome III in the wild-type (left) and tDNA delete (right) strains.

the same protein was mapped in the tDNA delete strain, we observed a significant reduction in Scc2 binding at these tDNAs. The levels dropped to those observed for the negative control *OCA4* except for the t8 tDNA, where the level dropped 2-fold but there was some residual Scc2 still present (Fig. 4A). The amount of Scc2 did not change at *CEN3* when the tDNAs were absent from the chromosome, indicating that the binding of Scc2 to the centromere was independent of the tDNAs.

Scc2, in association with Scc4, helps recruit the SMC proteins to chromatin (29, 32). Condensins localize to tDNAs and are necessary for the clustering of tDNAs in the nucleus (29, 30). We therefore mapped the binding of condensins at tDNAs on chromosome III using the hemagglutinin (HA)-tagged Brn1 subunit. In wild-type cells, the Brn1 profile was very similar to that previously observed for Scc2, with significant binding of Brn1 at specific tDNAs. Correspondingly, the binding of the condensins was significantly reduced at these sites upon deletion of the tDNA promoters (Fig. 4B).

Chromosome mobility on the tDNA-less chromosome. TFIIIC binding sites and tDNAs are described as chromosome-organizing clamps because of their consistent association with specific landmarks within the nucleus (54). The localization of tDNAs with the kinetochore is dependent upon condensins, while the interactions of tDNAs with nuclear pores in the G_2 phase of the cell cycle are dependent upon cohesins. These associations likely help tether the chromosome. Since loss of tDNAs from chromosome III led to a decrease in SMC proteins at these sites, we wondered if this loss would affect chromosome tethering and the mobility of the chromosome. To assess mobility, we

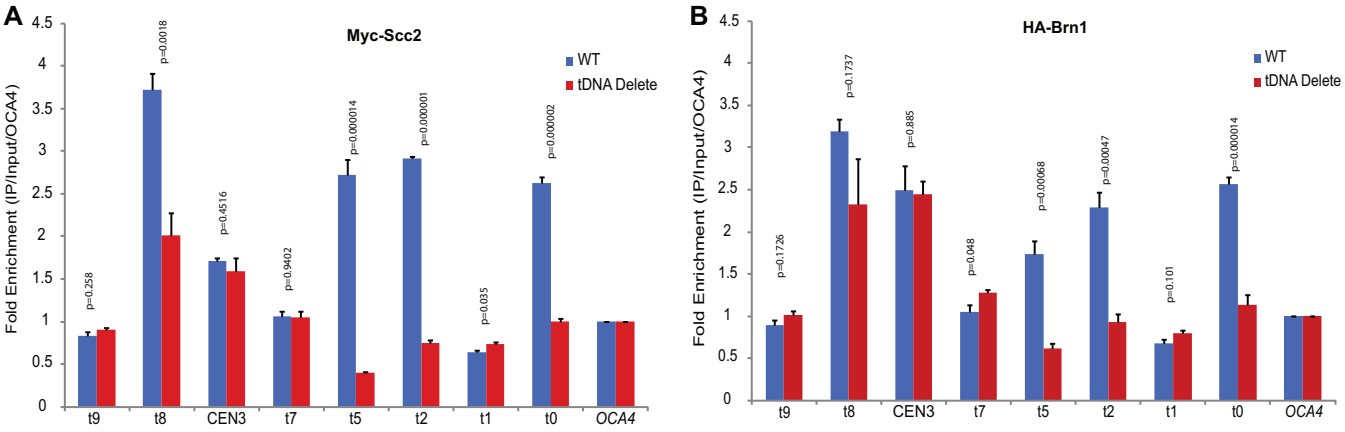

FIG 4 Scc2 and Brn1 binding at tDNAs on chromosome III. (A) ChIP-qPCR mapping of Myc-Scc2. The data show the distribution of Scc2 at specific sites along chromosome III in the wild-type and tDNA delete strains. The data are the results of two independent cross-links on which four IPs were performed. For each amplicon, the fold enrichment compared to input was first calculated, and the data were then normalized to the *OCA4* locus. An unpaired *t* test assuming unequal standard deviations (SD) was used to test for significance of differences between the wild-type and tDNA delete strains. (B) ChIP-qPCR mapping of HA-Brn1 and condensin. Fold enrichment and statistical significance were calculated in the same way as for the Scc2 ChIP and normalized to the *OCA4* locus. The error bars indicate SD.

fluorescently labeled specific sites on chromosome III and used them to monitor chromosome mobility in the wild-type and tDNA deletion chromosomes. The location of a point on the chromosome was mapped in three-dimensional space over a defined period in relation to another point within the nucleus—the spindle pole body (marked with the Spc29-red fluorescent protein [RFP] fusion protein)—and mobility was characterized by mean square distance (MSD) analysis as described previously (66–68). Six chromosomal loci across chromosome III were assayed (Fig. 5). These loci were tagged by inserting LacO arrays at the sites and monitored using LacI-green fluorescent protein (GFP) fusion protein-mediated fluorescence. Time-lapse movies of >35 individual unbudded cells (in the G_1 phase of the cell cycle) were imaged over the course of 10 min. Z-stack images of the cells were taken every 30 s during the time-lapse movie, and the MSD was calculated at each time point using the following equation: $\mathrm{MSD} = (X_{t+T} - X_t)^2 + (Y_{t+T} - Y_t)^2$, where X and Y are the coordinates of the fluorescent dot, T is the time lag, and t is the time. Using this information, MSD curves were generated for each locus in both the WT and tDNA delete strains (data not shown). For the wild-type chromosome III, *CEN3* was the most constrained locus (radius of constraint [Rc] = 415 nm), with loci located further from the centromere exhibiting greater mobility. For example, *LEU2*, which is approximately 30 kb from the centromere, had an Rc of 522 nm, while *HMR*, which is approximately 180 kb from the centromere, had an Rc value of 688 nm. This is consistent with previous data showing that the location of a locus in relation to the centromere is critical in determining its mobility, with loci closer to the centromere displaying decreased mobility compared to loci farther from the centromere (9, 68, 69). Comparison of the mobilities of segments in the wild-type and tDNA delete strains showed a small decrease in mobility in the tDNA delete strain at two sites (*SRO9* and *CEN3*). However, these differences were not statistically significant ($P = 0.15$ and 0.19). The data indicate that tDNAs are not major determinants in constraining chromosome arm motion or that they are a subset of the factors involved, and the redundancy precludes observation of their contribution.

tDNAs are not required for proper chromatin folding. tRNA genes have been proposed to affect chromatin fiber folding via the clustering of dispersed tRNA genes. The promoters in tDNAs are the binding sites for the transcription factor TFIIIC, and foci comprised of multiple TFIIIC-bound sites have been proposed to function in chromatin looping and folding (10, 39, 52–54, 57, 58, 70). If tDNAs are major drivers of chromatin folding and looping, then elimination of these loci from an entire chromosome should lead to changes in the folding of the chromatin fiber or result in changes in chromo-

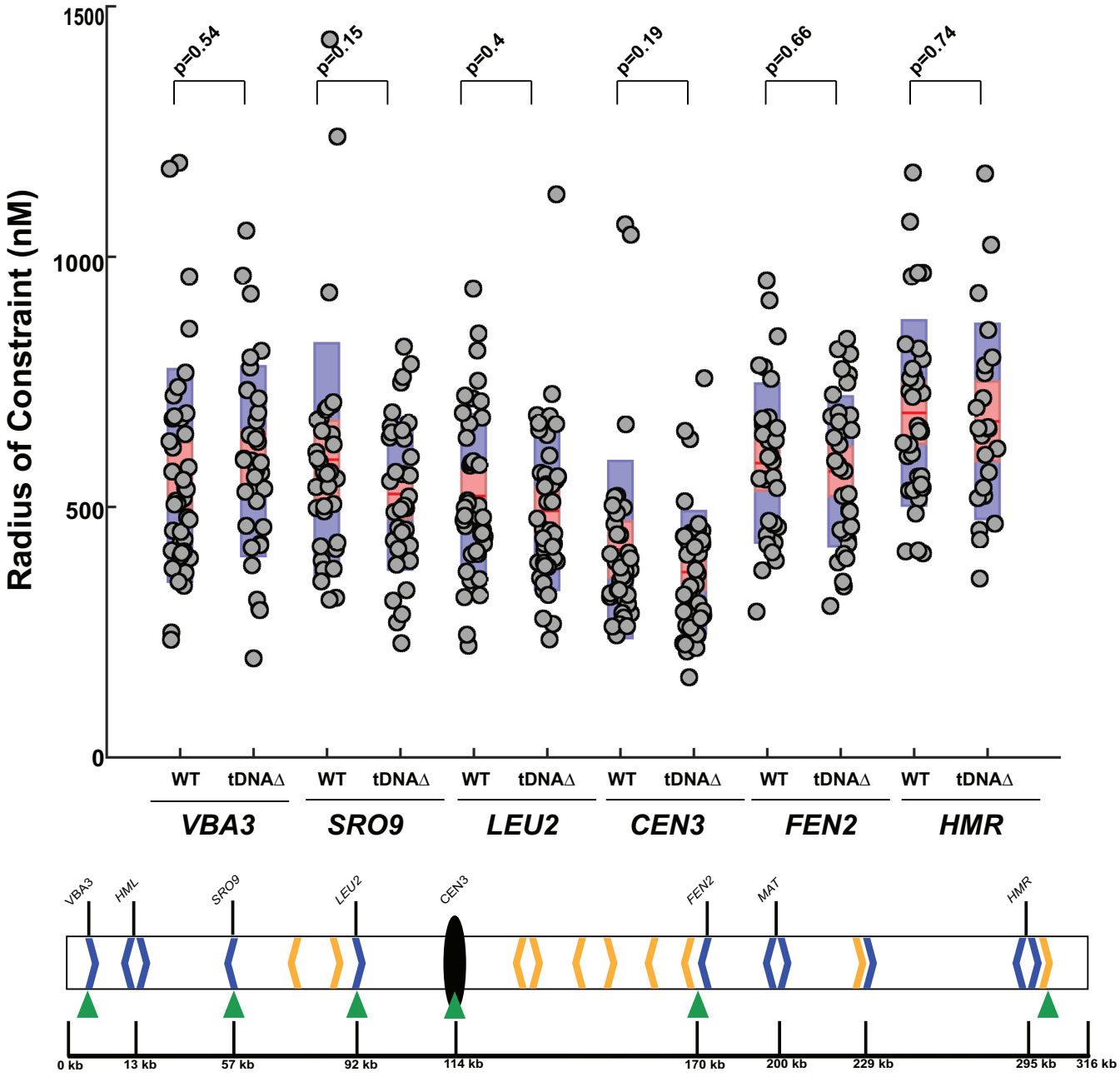

FIG 5 Effect of tDNA deletion on chromosome III mobility. Mean square displacement analysis of seven loci along chromosome III in wild-type and tDNA delete strains is shown. The box plots represent the data obtained from the MSD experiments. The components of the box plots are as follows: red lines, means; pink bars, 95% confidence intervals; purple bars, standard deviations; gray dots, individual values obtained from each cell analyzed. The arrowheads below the chromosome III schematic show the locations of the loci assayed. The Rc measurement was calculated from MSD graphs that were generated over the course of a 10-minute time-lapse movie. The experiments were the result of time-lapse images taken from at least 35 cells per locus assayed. A *t* test was used to determine the significance of differences observed between the wild-type and tDNA delete strains for each locus.

some packaging in the nucleus. We set out to determine the detailed three-dimensional organization of chromosome III lacking functional tDNAs. We used a modified chromosome conformation capture technique called Micro-C XL (71, 72). We chose Micro-C XL over HiC because it can capture both short 3D interactions and some long interactions, and the method is not dependent upon the distribution of restriction sites along the DNA. In brief, yeast cells were first cross-linked with formaldehyde and disuccinimidyl glutarate (DSG), and chromatin was then fragmented into nucleosomes via micrococcal nuclease digestion. The cross-linked, digested chromatin was ligated to

capture chromosomal interactions. Size-selected ligation products were then purified and subjected to paired-end high-throughput sequencing. The sequencing reads were mapped back to the reference genome to determine the interacting regions of the chromosome, as previously described. For each strain, two independent cross-linking experiments and ligations were performed, and QuASAR (quality assessment of spatial arrangement reproducibility) and Genome DISCO (differences between smoothed contact maps) were used to assess the reproducibility of the data. The two independent measurements both gave a score of >95%, confirming the reproducibility between the two biological replicates for the wild-type and tDNA delete strains. The reproducibility of the data was also analyzed by measuring contact probability over genomic distance, and the decay curves between replicates overlapped almost completely, which is consistent with our reproducibility measurements.

Overall, Micro-C maps for the wild-type and tDNA mutant strains both exhibited previously described features of yeast chromosome folding, with no difference in chromatin folding between the tDNA delete and wild-type strains. The chromatin interaction maps of chromosome IX showed that most Micro-C interactions occurred close to the diagonal in both strains, though there was significant variation in the density along the diagonal. The data clearly show ~2- to 10-kb contact domains (chromosomally interacting domain [CIDs]/topologically associating domains [TADs]) encompassing ~1 to 5 genes in both strains (Fig. 6A). We calculated the insulation score across bins, and a scatter plot of the insulation scores for wild-type and mutant strains was consistent with the conclusions that the overall architecture of chromosomes in the two strains was not altered (Fig. 6B).

Inspection of chromosome III in the wild-type and tDNA delete cells showed that these interaction domains persisted on the chromosome even upon loss of the tDNAs from chromosome III. The interaction decay curves for chromosome III were very similar in the wild-type and tDNA delete strains, indicating that the overall folding of the chromosome had not altered (Fig. 6C). There was no significant change in the contact frequency versus genomic distance in the two strains, indicating no local chromatin decondensation or change in chromatin-looping interactions.

We analyzed the contact frequencies of sites immediately adjacent to the 8 tDNAs on chromosome III in the wild-type and tDNA delete strains. At some sites, the loss of the adjacent tDNA did not alter long-range interactions at all, while at other sites there were small changes, though the significance of these remains to be elucidated (Fig. 6D).

Thus, tDNAs do not appear to be responsible for the general folding of the chromatin fiber and the CID/TAD architecture.

tDNAs affect CEN-CEN interaction frequency. While the overall folding of the chromatin fiber of chromosome III was not altered, Micro-C analysis identified changes in contact frequency at specific sites along chromosome III. In order to identify sites where contact frequency had changed, the contact maps were normalized by distance for the wild-type and tDNA delete strains (Fig. 7A). These matrices were used to identify differential contact sites (generated by dividing the tDNA delete matrix by the wild-type matrix). This analysis identified increased sites of contacts in the tDNA delete strain (shown in red) around the centromere and near the telomeres of chromosome III (Fig. 7B).

The 16 centromeres in yeast are in close physical proximity to one another and cluster adjacent to the spindle pole body (7, 73, 74). These CEN-CEN interactions are readily captured by chromosome conformation capture (3C) methods, including HiC (10, 71, 75), and are recapitulated in this study in the W-303 strain background. Interestingly, compared to the wild-type strain, the centromere of chromosome III in the tDNA delete strain showed an increased frequency of interactions with the other centromeres. Focusing on the 50-kb pericentric region of each chromosome, we found that most CEN-CEN interactions were minimally affected by the loss of chromosome III tDNAs. For instance, interactions between the chromosome XVI centromere and the remaining centromeres showed that interactions between *CEN16* and the majority of

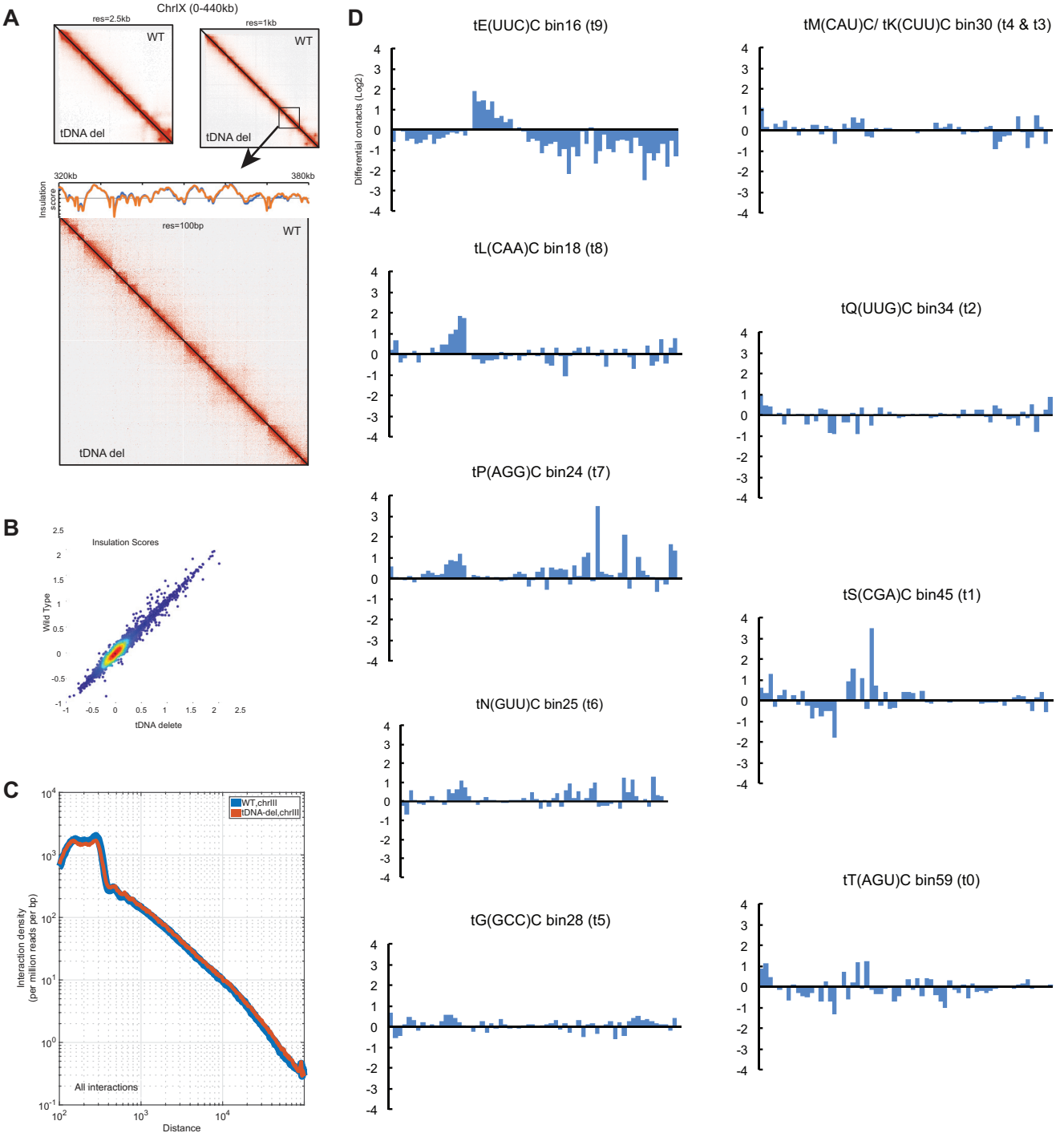

FIG 6 Micro-C interaction plots of chromosome III. (A) Snapshot of chromosome IX at 2.5-kb resolution and 1-kb resolution. The wild type and tDNA delete mutant are shown in the contact matrices. The bottom matrix is a view of a segment at 100-bp resolution, and the insulation scores are plotted above the contact matrix. The insulation score is the value obtained by calculating the number of contacts within a 10-kb-by-10-kb sliding window using the 1-kb-resolution contact matrix. The local minima identify boundaries that help demarcate CIDs. (B) Scatter plot of insulation scores showing that there was no change in insulation strength between the wild-type and tDNA delete strains. (C) Interaction decay curve for chromosome III showing that there were no significant changes between the wild-type and tDNA delete strains. (D) Circular chromosome conformation capture (4C)-type contact graph using a region immediately adjacent to the deleted tRNA gene. The 1D contact matrix at 5-kb resolution was plotted. The *y* axis is the $\log_2$ ratio of differential contacts between the wild-type and tDNA delete strains.

centromeres remained unchanged but that there was an ~20% increase in interaction strength between *CEN16* and *CEN3* when chromosome III lacked tDNAs (Fig. 7C).

This increase in *CEN3* interaction was not confined to *CEN16*. When the same analysis was performed using *CEN3* as an anchor, we observed increased frequency of

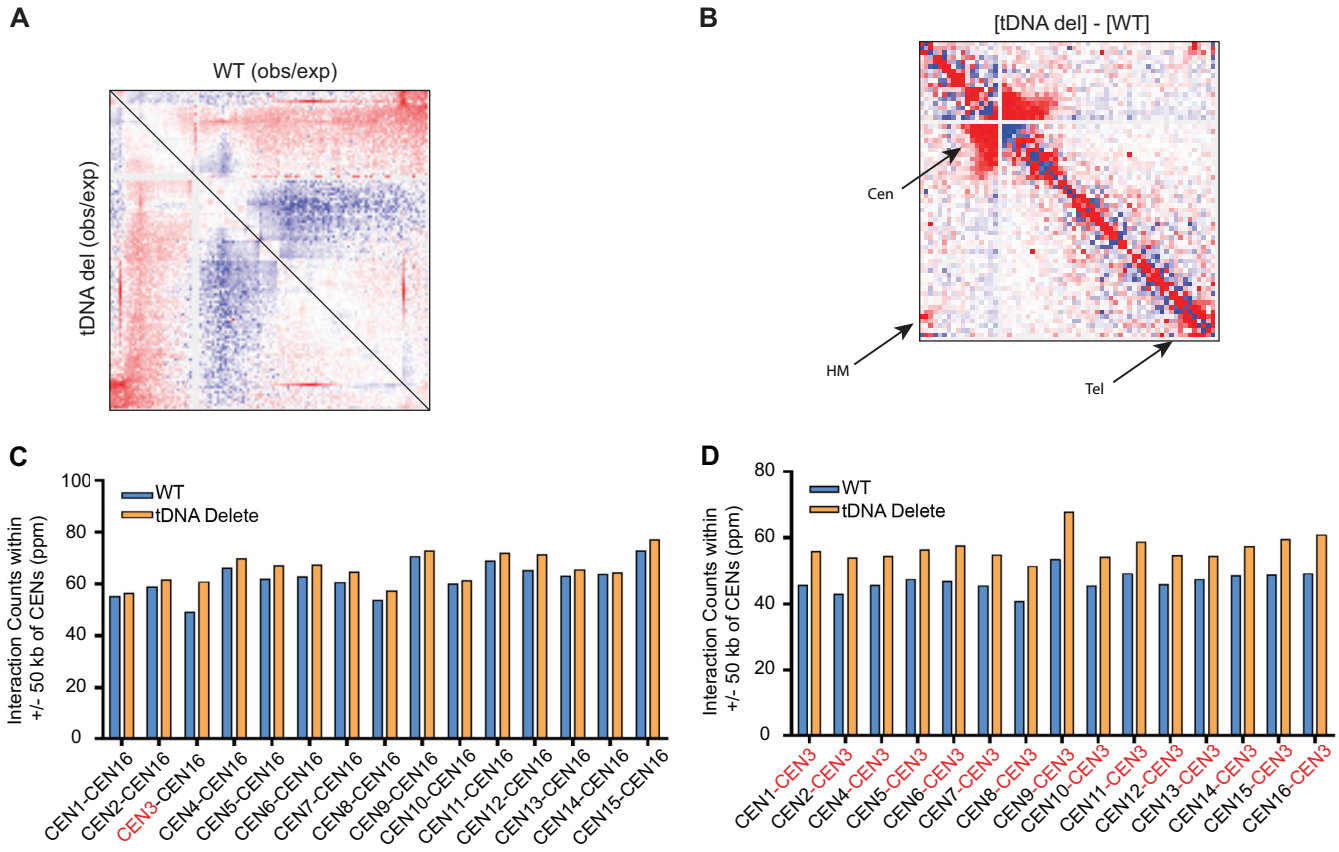

FIG 7 Micro-C analysis of the centromeres. (A) Contact map of chromosome III for the wild-type and tDNA delete strains normalized by distance (obs/exp, observed/expected). (B) Differential contact maps were generated by dividing the tDNA matrix by the wild-type matrix. Increased contacts in the tDNA delete strain are shown in red, and reduced contacts in the tDNA delete strain compared to the wild-type strain are shown in blue. Tel, telomere; Cen, centromere; HM, *HML* and *HMR*. (C and D) Graphs quantifying *CEN-CEN* interactions. (C) Graph examining the interaction of *CEN16* with all other centromeres. The *x* axis shows the interaction counts of a 50-kb segment centered on each centromere. (D) Graph examining the interaction of *CEN3* with all other centromeres. The *x* axis shows the interaction counts of a 50-kb segment centered on each centromere. The increase in the CEN3-CEN interactions in the tDNA delete strain was significantly greater ($P = 1.22 \times 10^{-14}$) than the values of all CEN16-CEN interactions (excluding CEN16-CEN3).

interactions between *CEN3* and all of the other chromosomal centromeres in the tDNA delete strain (Fig. 7D). Most of the interaction counts increased approximately 20% compared to the WT, with the greatest increase seen at *CEN3-CEN9*. The increase in the CEN3-CEN interactions in the tDNA deletion strain was significantly greater ($P = 1.22 \times 10^{-14}$) than the values of all CEN16-CEN interactions (excluding CEN16-CEN3). These results show that upon deletion of all tDNAs across chromosome III, interchromosomal interactions increase between *CEN3* and the other centromeres, suggesting that functional tDNAs likely antagonize CEN-CEN associations during interphase.

We next measured chromosome loss rates of wild-type and tDNA delete diploid cells. We first constructed homozygous diploid cells containing *URA3*, *TRP1*, and the *MAT* locus located on chromosome III (in both the wild-type and tDNA delete strains). Single diploid colonies were grown for 20 doublings in yeast extract-peptone-dextrose (YPD) medium, and approximately 10^7 cells were plated onto 5-fluoroorotic acid (5-FOA) plates to measure the number of cells that had become *URA3* negative. Cells could have become uracil auxotrophs by gene mutations or via loss of the chromosome. These two types of mutants could be distinguished by replica plating the 5-FOA-resistant colonies onto plates lacking tryptophan or by checking for the appearance of MATα pseudohaploid cells. The cells unable to grow on medium lacking tryptophan and also able to mate were counted, and chromosome loss rates were calculated by dividing the number of these colonies by the total number of cells plated.

In wild-type cells, the loss rate for chromosome III was 4.08×10^{-5}, which is in agreement with previous reports (76). The loss rates for the tDNA delete chromosome decreased slightly to 3.26×10^{-5}, suggesting that loss of tDNA slightly helped stabilize the chromosome ($P = 0.02$).

tDNAs play a role in *HML-HMR* long-range association. The silent loci *HML* and *HMR* reside on chromosome III separated by approximately 300 kb along the linear chromosome. However, the *HML* locus, located 11 kb from *TEL3L*, is in close three-dimensional proximity to the *HMR* locus, located 23 kb from *TEL3R*. This long-range interaction has previously been detected using both live-cell microscopy and HiC analysis (20, 75, 77), and we recapitulated this finding in the Micro-C experiment with the wild-type strain (Fig. 8A). Comparing wild-type cells to the tDNA delete strain, we noticed that the interaction of *HML* with *HMR* was slightly altered in the tDNA delete strain. In wild-type cells, there was an interaction between *HML* and *HMR*; this interaction zone became less defined and more diffuse upon deletion of the tDNAs, and a slightly increased interaction frequency was observed across a broader region of the end of chromosome III. While *HMR* still interacted with *HML* in the deletion strain, it appeared to also display interactions with other loci (including *TEL3L*). Similarly, the segment containing *HML*/*TEL3L* showed increased interactions with *TEL3R* rather than being restricted to interacting with sequences at *HMR*. These results suggest that deletion of chromosome III tDNAs subtly perturbed *HML-HMR* long-range interactions.

Given that Micro-C measures population averages of stable long-range interactions, we decided to measure *HML-HMR* interactions in live cells using fluorescence microscopy. We wished to determine if the tDNAs influenced *HML-HMR* interactions. We generated a strain with multiple Lac operator sequences inserted adjacent to *HMR* (at the *GIT1* gene) and multiple copies of the Tet operator sequences inserted adjacent to *HML*. Expression of the fusion proteins cyan fluorescent protein (CFP)-LacI and yellow fluorescent protein (YFP)-TetR in this strain enabled us to visualize these loci in living yeast by fluorescence imaging. The distance between *HML* and *HMR* was then measured in the wild type and a strain lacking the t0 tDNA (Fig. 8B). We found that in wild-type cells, *HML* was in close proximity to *HMR*. Consistent with our expectations, deletion of Sir proteins resulted in separation of these loci, validating the assay. Importantly, when we eliminated the t0 tDNA, it led to a change in the distance between *HML* and *HMR* compared to wild-type cells, with the median distance between *HML* and *HMR* increasing upon deletion of the tDNA. Given the presence of outliers in the data, we used a Mann-Whitney U test to determine statistical significance between the wild type and the mutant. With approximately 300 cells for the wild-type and tDNA delete strains, we observed a *P* value of 3.1e−14, showing that the differences observed between the two strains were significant. Closer analysis of the plot indicated that upon deletion of the tDNA, there was heterogeneity in the distances between the two loci and a continuum of values. Thus, there were cells where the two loci were in very close proximity, as well as cells where the two loci were further apart. It should be noted that the HiC approach and the microscopy method to measure proximity are inherently different and distinct; each method provides a different type of information, and each approach has specific limitations. Use of long arrays bound tightly by repressor proteins that dimerize may influence chromatin architecture and fluorescence measurements (78). Similarly, the HiC-based methods are influenced by indirect cross-linking, especially in regions of condensed heterochromatin and nuclear substructures, like sites near centromeres and the nuclear envelope (79–81).

tDNA t0 is necessary for the recruitment of cohesins to the silenced loci, and the SMC proteins are necessary for long-range *HML-HMR* interactions (20). However, not all tDNAs are equivalent in their ability to recruit cohesins to the silenced loci (43, 82, 83). We therefore inquired if tDNAs that are unable to recruit cohesins are able to restore long-range association between *HML* and *HMR*. We replaced *HMR* $tDNA^{THR}$ (t0) with $tDNA^{THR}$ (NL1) from chromosome XIV. This tDNA has sequence identical to that of the t0 tDNA in the body of the gene and therefore has BoxA and BoxB promoter sequence

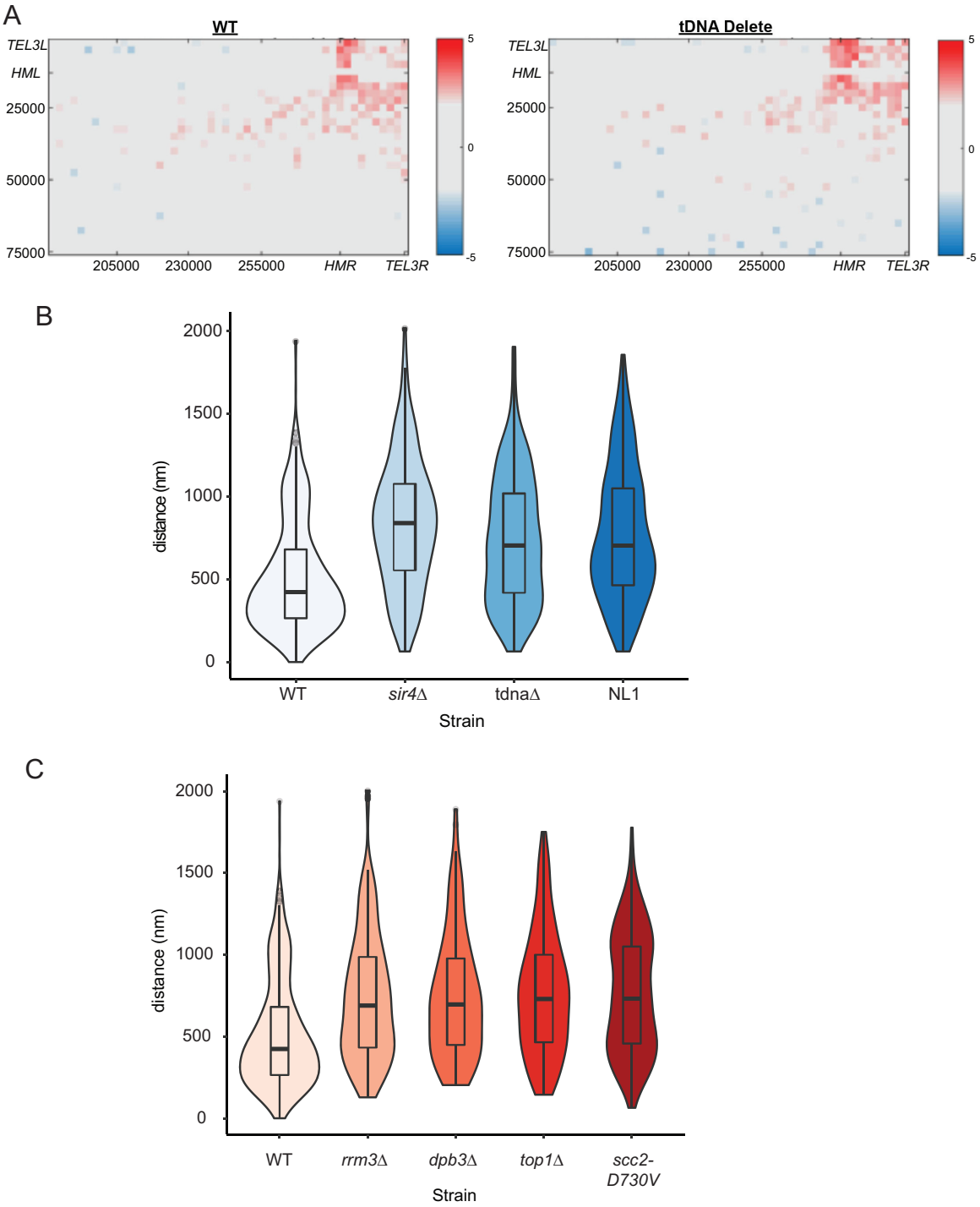

FIG 8 Long-range *HML-HMR* association. (A) Deletion of tDNAs on chromosome III leads to a change in *HML-HMR* interaction as measured by Micro-C. The heat maps display the interaction profiles between segments on chromosome III that include *HML* and *HMR* (obtained from the Micro-C data). Increased interactions are denoted by red, and decreased interactions are denoted by blue. The data are displayed in a $\log_2$ format. The *x* and *y* axes show the region of the chromosome displayed on each axis of the heat map. (B) Deletion of tDNA t0 leads to perturbation of *HML-HMR* long-range association. The violin plots show data on the distances between *HML*::TetR-YFP and *HMR*::CFP-LacI foci in asynchronously growing strains. Mann-Whitney U tests were performed to determine statistical significance between the wild type and the various mutants. Wild type, $n = 305$; *sir4*Δ strain, $n = 134$ ($P = 6.7e{-}16$); tDNA t0Δ strain, $n = 317$ ($P = 3.1e{-}14$); t0Δ:NL1 strain, $n = 330$ ($P = 2.2e{-}16$). The dark horizontal lines represent the median distances. The data for *sir4*Δ are shown as a control and are the same as those in reference 20. (C) Replication repair proteins are necessary for *HML-HMR* interactions. Violin plots of the distance between TetR-YFP and CFP-LacI foci in a given wild-type or mutant strain are shown. *rrm3*Δ, $n = 208$ ($P = 4.8e{-}12$); *dpb3*Δ, $n = 134$ ($P = 1.7e{-}10$); *top1*Δ, $n = 139$ ($P = 4.2e{-}12$); *scc2D730V*, $n = 188$ ($P = 1.9e{-}14$). The data for the *scc2D730V* allele are shown as a control and are the same as those in reference 20.

and spacing identical to that of tDNA t0. However, sequences flanking this tDNA are distinct, and the NL1 tDNA is unable to recruit/bind cohesins (82, 83). The NL1 tDNA has reduced binding of TFIIIC and a narrower nucleosome-free region, as well (62, 84). This tDNA also has reduced nucleoporin binding and reduced histone turnover frequency (61, 85). When we replaced a 300-bp t0 tDNA-containing fragment with a 300-bp NL1 tDNA-containing fragment, we found that the NL1 tDNA was not able to robustly restore long-range *HML-HMR* interactions, suggesting that tDNA-mediated local chromatin organization might be necessary for these long-range interactions.

Replication fork pausing at tDNA mediates long-range chromosomal interactions. We had previously shown that DNA double-strand repair proteins help deposit cohesins at the silenced loci, which then leads to homology-dependent long-range interactions between *HML* and *HMR* (19, 20). Since we had discovered that a specific tDNA helped in the clustering of *HML* and *HMR*, we wished to know the mechanism by which this phenomenon occurred. Replication fork pausing/stalling is observed at many tDNAs. It results in the deposition of γH2A at the tDNA, which is necessary for fork recovery from the pause/stall (20, 29, 86–90). Rrm3 and topoisomerases play a role in the recovery of stalled replication forks at protein-bound sites in the genome, such as tDNAs (88, 91, 92). Therefore, we analyzed the effects of these mutants on *HML-HMR* long-range association. The data show that deletion of Rrm3, as well as mutants in the DNA polymerase ε subunit Dpb3 and the topoisomerase Top1, lead to a statistically significant decrease in *HML-HMR* long-range association (Fig. 8C). Thus, the presence of a tDNA, as well as normal Rrm3, Top1, and Dpb3 function, is necessary for the establishment or maintenance of the long-range association between *HML* and *HMR*.

tDNA enhances epigenetic gene silencing at clustered *HML-HMR*. Since the tDNA is necessary for the long-range clustering of the silenced domain, we wondered if reduction in clustering had any effect on gene silencing. We asked whether tDNA-mediated loss of *HML-HMR* interactions affected gene silencing at *HML* and *HMR*. Silencing can be assayed by insertion of reporter genes within or immediately adjacent to the silenced domains. In wild-type yeast, when a reporter gene is inserted immediately adjacent to these loci, the gene is metastably silenced. A cassette containing an H2B (*HTB1*) promoter driving *HTB1-EYFP* was integrated to the right of *HML*, while a cassette containing the *HTB1* promoter driving *HTB1-ECFP* was integrated to the left of *HMR*. In addition, on chromosome XV, a cassette containing an *HTB1* promoter driving *HTB1*-mCherry was integrated as a control euchromatic marker (93). The *HTB1*-mCherry gene was active in all the cells in the population. The *HML*::*YFP* and *HMR*::*CFP* reporter genes are present immediately outside *HML* and *HMR* but reside in a region bound by Sir proteins (4, 22). These genes adopt one of two expression states, either active or silent. For visualization, single cells were placed on microfluidic plates and monitored continuously by fluorescence microscopy. Fluorescent signal from each individual cell was recorded every 40 min over a period of ~24 h. This allowed us to trace the lineage of each daughter from the founder cell and score the cells according to the expression of the reporter genes at *HML* and *HMR*. Cell lineage trees were traced, and each cell in the lineage was assigned a positive or negative value for expressing each reporter as it underwent cell division (Fig. 9A).

We initially analyzed the silencing of the reporter genes in the wild-type strain. Consistent with previous data (93), reporters at *HML* and *HMR* were regulated so that the reporters maintained their activity state over many generations and occasionally switched to the opposite expression state. Once they switched, they maintained the new state for several generations. Furthermore, when one reporter was active, the other was also more likely to be active, suggesting long-range coordination between *HML* and *HMR*, though this coordination is not absolute.

We next investigated silencing of the reporters in a strain where chromosome III lacked all the tDNAs. In this strain, the reporter at *HMR* was active more often than in the wild-type strain. While the effect was not as pronounced, the same effect was also observed at *HML* (Fig. 9A, tDNA delete). Furthermore, the silenced state was less stable

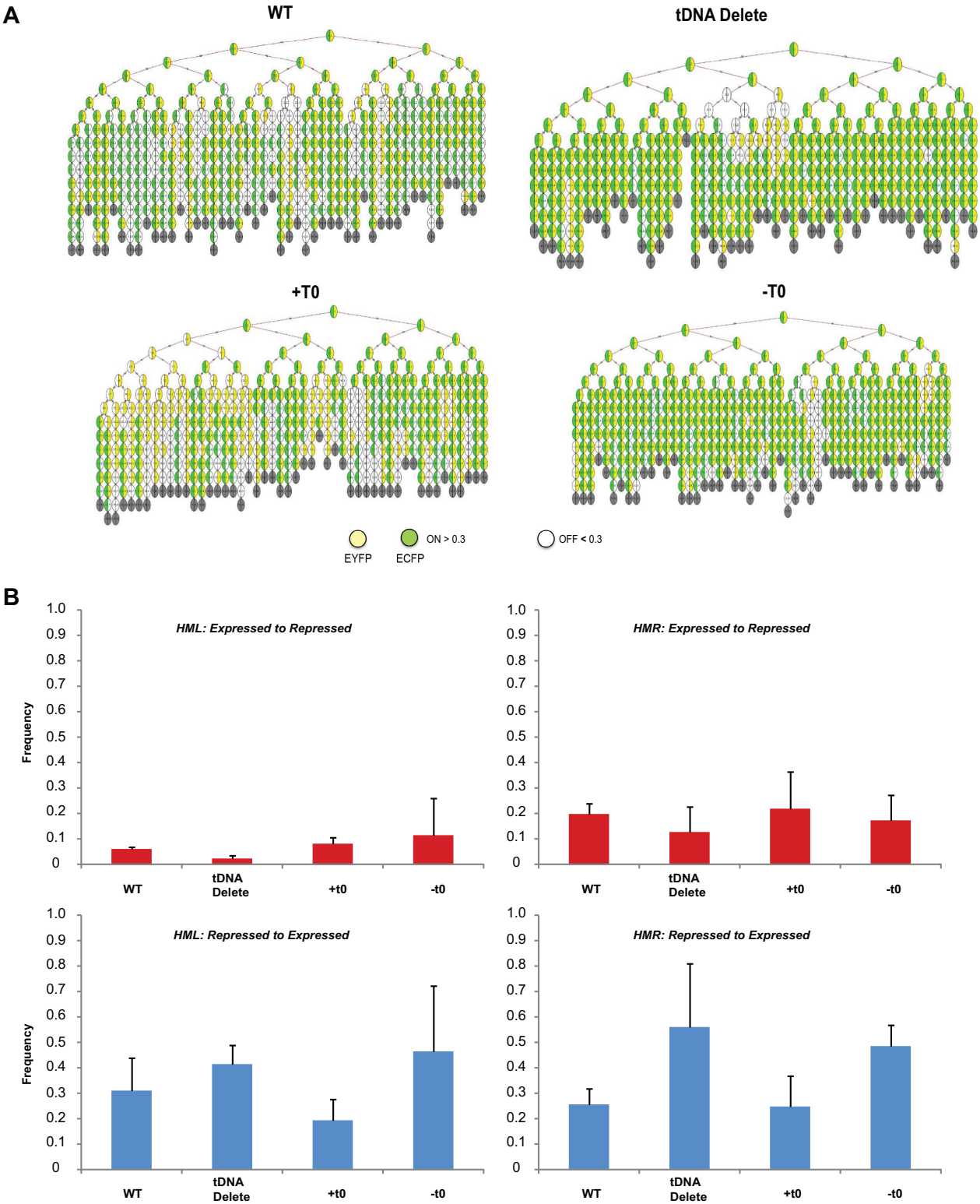

FIG 9 Silencing of reporter genes at *HML* and *HMR*. (A) tDNAs on chromosome III modulate silencing of reporter genes at *HML* and *HMR*. Representative lineage trees of the different strains that were analyzed are shown. Wild type refers to a strain containing all the tDNAs on chromosome III. tDNA delete refers to a strain lacking all of the tDNAs on chromosome III; +T0 refers to chromosome III containing only the T0 tDNA; −T0 refers to chromosome III lacking only the T0 tDNA. The expression of *HML::EYFP* or *HMR::ECFP* in each generation of cells was monitored and quantitated and is indicated by the presence of their respective colors in the cells of the tree. (B) Deletion of tDNAs on chromosome III leads to a change in the maintenance of silencing at *HML* and *HMR*. The graphs quantify the changes in expression state of *HML::EYFP* and *HMR::ECFP* between generations in the different genotypes studied. Expressed-to-repressed transitions identify reporters that were expressed in one generation but not expressed in the next. Repressed-to-expressed transitions represent reporter genes that were not expressed in one generation but were expressed in the next. The error bars indicate SD.

TABLE 2 Statistical analysis of differences in expression of HML::EYFP and HMR::ECFP in the wild-type and tDNA delete strains

	Frequency of[a]:			
	HMR		HML	
Strain	Expressed to repressed	Repressed to expressed	Expressed to repressed	Repressed to expressed
WT	0.2 (0.019)	0.25 (0.031)	0.06 (0.005)	0.3 (0.075)
tDNA delete	0.13 (0.057)	0.56 (0.145)	0.02 (0.006)	0.41 (0.041)
t0+	0.22 (0.085)	0.25 (0.070)	0.08 (0.014)	0.19 (0.049)
t0−	0.18 (0.049)	0.48 (0.041)	0.11 (0.072)	0.46 (0.12)

[a]Numbers in parentheses are standard deviations.

and switched to the active state more often. This suggests that silencing at these loci is influenced by the tDNAs.

While expression states at both *HML* and *HMR* were stably inherited, the transcriptional state did flip in daughter cells (Fig. 9B). An expressed-to-repressed transition was a less frequent event than the repressed-to-expressed transitions regardless of genotype. This is not entirely surprising, since the reporter genes were inserted immediately outside the two silencers in a zone where the silent state is metastable (94, 95). However, when analyzing the repressed-to-expressed transitions, we saw a discernible difference in the frequency of the expression of the reporter genes at *HMR*. The full tDNA delete strain showed an increased frequency of cells undergoing the transitions at *HMR* compared to wild-type cells, and the inverse was seen for the expressed-to-repressed transition (Table 2).

Given that the transcription states of the reporters were affected at both *HML* and *HMR* in a strain containing full tDNA deletions on chromosome III, even though only *HMR* has a tDNA adjacent to it, we decided to focus on the tDNA (t0) that resides immediately adjacent to *HMR* and functions as an insulator at *HMR*. Importantly, t0 lies to the right of *HMR* while the reporter gene lies to the left of *HMR*, so any effect of t0 on the transcriptional state of the reporter is not due to the barrier function of the tDNA.

To test whether t0 is necessary for regulating silencing states at *HML* and *HMR*, we built a strain where only t0 was deleted on chromosome III (t0−). The lineage tree showed that the strain behaved similarly to the strain lacking all tDNAs in that both reporters were active most of the time and rarely switched to the repressed state. Like the full tDNA delete strain, the t0− strain showed an increased frequency of cells undergoing the transitions at both *HML* and *HMR* compared to the wild-type strain, where a reporter gene that was not expressed in one generation was more likely to be expressed in the next generation.

Alternatively, to determine if the t0 tDNA was sufficient to mediate silencing effects at *HML* and *HMR*, we constructed a strain lacking 9 of the 10 tDNAs on chromosome III and where t0 was the only tDNA still present at its normal location adjacent to *HMR* (t0+). Again, we monitored expression of the reporters at *HML* and *HMR* in this background. The lineage tree showed that the strain behaved similarly to the wild-type strain in that both reporters were silent more often than for the full tDNA delete and t0− strains and inherited the silent state with greater fidelity.

Taken together, the data suggest that deletion of tDNAs on chromosome III had an effect on the ability of *HMR* to interact with *HML* and that diminution of this clustering led to an alteration in the stability of the silenced state at these loci.

DISCUSSION

tDNAs are middle repetitive DNA sequences (i.e., moderately repetitive DNA [usually rRNA and tRNA genes] [140]) scattered across all 16 chromosomes, and their primary function is the synthesis of tRNAs. Here, we show that tDNAs affect local chromatin structure, which then impinges on chromosome architecture. tDNAs (i) affect chromatin structure by maintaining local nucleosome-free regions along the fiber and precisely positioned nucleosomes immediately outside the tDNAs, (ii) recruit cohesins and

condensins, (iii) affect nuclear architecture by influencing centromere clustering, and (iv) alter heterochromatin clustering, leading to changes in the fidelity of inheritance of gene silencing.

The binding of specific proteins, such as CTCF, to a site on the DNA can affect nucleosome positions over long distances (96). Nucleosome depletion at the gene and positioned nucleosomes flanking the gene are hallmarks of tDNAs (22, 24, 25, 35, 61, 97–100). Our data show that loss of the tDNA promoters affects only nucleosome positions in the immediate vicinity of the tDNA. The nucleosome-positioning effects mediated by the tDNA-bound transcription factors TFIIIC and TFIIIB are not transmitted over long distances.

tDNAs, SMC proteins, and chromatin folding. The SMC proteins are involved in higher-order chromosome organization in all eukaryotes and have been extensively mapped. tDNAs are binding sites for all three classes of SMC proteins (cohesins, condensins, and SMC5 and SMC6 proteins involved in DNA repair [repairsins]), the SMC protein loaders Scc2 and Scc4, and the meiotic Rec8 SMC protein (28, 29, 32, 101–105). Given these intimate connections between tDNAs and the SMC proteins, our data indicate that loss of the tDNA promoters does lead to loss of SMC proteins from tDNAs, but this effect is tDNA specific, since we do not see a loss of SMC proteins from centromeres or of Scc2 from other sites in the genome. Surprisingly, the loss of Scc2 and Brn1 from tDNAs does not affect chromatin folding. While clustering of tDNAs in the nucleus (as measured by fluorescence microscopy) is dependent upon the SMC proteins (54, 70), the precise contribution of tDNAs in this process remained unclear. Our Micro-C analysis suggests that tDNAs play a minor role in chromatin folding and tethering to nuclear substructures, since we observed only subtle changes in contact frequency across the chromosome and small effects on chromosome loss rates. It is likely that tDNA-independent SMC protein binding sites mask the tDNA-mediated effects. SMC proteins bind only half of the tDNAs in the nucleus, and only a third of the SMC protein binding sites localize at or near tDNAs (29). The lack of phenotype is also consistent with previous data that showed that a reduction in the levels of the SMC proteins does not affect the properties of the chromosome arm (106). Recently a synthetic yeast chromosome III was generated and characterized (107, 108). The synthetic chromosome lacks repetitive sequences, such as TY elements, long terminal repeats (LTRs), and tRNA genes. The 3D structure of the chromosome was determined using HiC, and the data show that there were no major differences between this chromosome and the wild-type chromosome except for a decrease in the length. While the chromosome lacks multiple elements, the three-dimensional folding data are consistent with our conclusions from the Micro-C analysis that the same chromosome lacks only tDNAs.

While it is possible that redundancy of structural elements masks tDNA-mediated effects on chromatin folding, it is also possible that chromatin folding is driven by underlying DNA sequence-mediated nucleosome organization and not tDNA-mediated long-range interactions. The yeast chromosomes have isochores with G-C-rich, gene-rich R band segments alternating with AT-rich G band segments (109, 110), which exhibit different functional properties and chromosome conformation (111, 112). Chromosome III has a G-C segment from kb 20 to 100 on the left arm, followed by an A-T-rich central segment from kb 100 to 200 on the right arm and then a second G-C-rich segment from kb 200 to 290 on the same arm. In this scenario, the underlying A-T-rich DNA sequence likely plays a dominant role in the three-dimensional folding of chromatin. tDNAs are often syntenic along chromosomes (39, 113), and it is possible that these positions have been selected for optimal gene activity rather than being involved in long-range chromatin loop formation (114). Thus, while the A-T-rich isochore is structurally and functionally distinct (75, 115, 116) and is the region rich in tDNAs (Fig. 1), our results suggest that the tDNAs do not play a significant role in either tethering of this isochore or the overall folding of the segment. The tDNA clustering

observed by microscopy could simply be a function of conservation of tDNA positions along the chromatin fiber.

tDNAs and centromere clustering. Chromosome tethering to nuclear substructures enables nuclear organization (1, 114), and centromeres and telomeres, along with their associated proteins, play a key role in this process (7, 9, 10, 12, 15, 16, 73, 117–120). All sixteen centromeres cluster together in a ring around the membrane-embedded spindle pole body. The centromeres are tethered to the spindle pole body via direct interactions between kinetochore-associated proteins and the spindle pole body-associated microtubules in interphase (7, 73, 75, 117). Other factors are likely to influence this phenomenon but remain unknown. tDNA density is almost 2-fold higher in the pericentric region of *S. cerevisiae* chromosomes, including chromosome III (121). While tDNAs have been shown to help tether centromeres to the spindle axis during mitosis (121), in interphase nuclei, the loss of tDNAs results in increased interactions between the clustered centromeres. The physical presence of tDNAs in the pericentric region could interfere with the close packaging of centromeres during interphase. This could be due to transcription-mediated effects, since tRNA genes are highly active. In *Schizosaccharomyces pombe*, mutations that reduce tDNA transcription result in increased tDNA association with the kinetochore and increased chromosome condensation during mitosis. Furthermore, tDNA association with kinetochores increases when these genes become inactive (55). Thus, tDNA clustering at sites of active tRNA transcription near centromeres could hinder centromere-centromere interactions during interphase, while a decrease in tDNA transcription during mitosis could help tether centromeres to the spindle axis during mitosis (121). This would also explain the observation that the chromosome with tDNA deleted had a slightly lower chromosome loss rate.

An alternative, though not mutually exclusive, possibility is based on the observation that transcriptionally active tDNAs interact with nuclear pores in the G_2/M phase of the cell cycle (4, 122, 123). It is thus possible that there is competition between pericentric tDNA–nuclear-pore interactions in opposition to centromere-centromere interactions. In this scenario, the loss of tDNA tethering to the nuclear pore would provide the centromere greater freedom of movement, thus enabling closer centromere-centromere interactions.

tDNA effects on *HML-HMR* interactions and the inheritance of gene silencing. Gene silencing is primarily a function of the Sir proteins, though numerous other factors influence the process (124). Protosilencers are sequence elements that on their own are unable to silence a gene but when located near a silencer increase the efficiency of silencing (125, 126). Our demonstration that tDNA affects silencing of a reporter adjacent to the silent *HMR* domain suggests that tDNAs function as protosilencers. Our data suggest that tDNA-mediated clustering of silent loci might be important in the silencing of these loci and that the loss of long-range association might reduce the efficient inheritance of the silent state. This is analogous to the observations that gene clustering at active chromatin hubs and transcription factories increases the efficiency of transcription, as well as the data showing that telomere clustering increases the efficiency of silencing at subtelomeric sequences (127).

This unexpected observation also raises the question of how tDNAs might influence long-range *HML-HMR* interactions. tDNAs, including the tDNA next to *HMR*, are sites of replication slowing/pausing (86, 87, 91, 128–130). The tDNA adjacent to *HMR* is a site of replication fork pausing (89, 131). We recently showed that long-range *HML-HMR* interactions require homologous sequences to be present at these loci (19, 20), and we now show that mutations in replication-coupled homologous recombination repair proteins, including the SMC proteins, Rrm3, Top1, and Dpb3, lead to a reduction in *HML-HMR* interactions. Based on the accumulated data, we posit that replication fork slowing/pausing results in the deposition of γH2A and SMC proteins at tDNAs, followed by a homology search leading to *HML-HMR* interactions. The re-formation of silenced chromatin following replication precludes the eviction of γH2A (132), thereby stabilizing SMC protein binding, which then maintains the long-range *HML-HMR* association.

The tDNAs thus help initiate a network of interactions mediated by the SMC proteins and the Sir proteins, leading to *HML-HMR* association and chromosome folding. We posit that a series of transient interactions during replication aid in setting up the final optimal nuclear architecture found in the interphase nucleus.

In conclusion, tDNAs primarily affect local chromatin structure. Each tDNA affects nucleosome positions and protein binding in its immediate vicinity. These local perturbations functionally and structurally interact with neighboring regulatory regions, resulting in tDNA-mediated pleiotropic effects. In some instances, tDNAs affect the expression of neighboring Pol II-transcribed genes by the phenomenon of local tgm silencing. In another context, tDNA-mediated replication pausing results in the establishment of long-range heterochromatin interactions, which then influence the inheritance of silencing states at these loci.

MATERIALS AND METHODS

Yeast strains and primers. Tables 3 and 4 list the yeast strains and the primer sequences that were used in this study.

MNase-seq. MNase-seq experiments were carried out as previously described (25). In brief, isolated nuclei were digested with MNase to mononucleosomes. Paired-end sequencing libraries were prepared (Illumina). Paired reads (50 nucleotides [nt]) were mapped to the reference genome (SacCer2) using Bowtie-2 (133–135). For analysis of nucleosome occupancy (coverage) at tDNAs, both across the genome and on chromosome III, tDNAs were aligned on their start sites or at the deletion points. Data sets were normalized to their genomic average (i.e., 1) using only DNA fragments in the 120- to 180-bp range. In one experiment, mononucleosomal DNA was gel purified, but not in the replicate, in which short fragments (<120 bp) derived from digestion of the TFIIIB-TFIIIC complex at tDNAs (97) were observed.

ChIP-seq and RNA-seq. Chromatin immunoprecipitation reactions were performed essentially as described above, but elution of the precipitated DNA from protein A/G beads was carried out with two successive washes in 175 μl of 0.1 M $NaHCO_3$-1% SDS; 50 μl of each input sample was diluted to 350 μl with the elution buffer. NaCl was added to a final concentration of 0.2 M, and cross-links were reversed with an overnight incubation at 65°C in a Thermomixer (Eppendorf). All samples were treated with 60 μg of RNase A (Sigma) at 37°C for 60 min, followed by proteinase K (Roche) treatment at 50°C for 60 min. DNA was purified with successive phenol chloroform and chloroform extractions, followed by precipitation with 2 volumes of ethanol and 50 μg of glycogen (Roche).

The ChIP and input DNAs were spun, washed with 70% ethanol, and resuspended in deionized water. DNA quantitation was performed using a Qubit double-stranded DNA (dsDNA) HS assay kit prior to confirmation by qPCR.

Libraries for ChIP-seq were prepared at the Functional Genomics Laboratory, University of California—Berkeley (UC Berkeley), and sequenced on an Illumina HiSeq 4000 at the Vincent J. Coates Laboratory at UC Berkeley.

For RNA-seq, yeast strains JRY2334 and JKY690 were grown in duplicate in 50 ml YPD to a cell density of 6×10^6 to 7×10^6 cells/ml, spun, washed in 25 ml phosphate-buffered saline (PBS), divided into 4 aliquots per culture, and transferred to 1.5-ml microcentrifuge tubes. The cell pellets were flash frozen in liquid N_2 and transferred to −70°C. RNA library preparation and sequencing for RNA-seq were performed by ACGT, Inc., Wheeling, IL.

Transcript abundances were estimated using Kallisto (136). Differential analysis of gene expression data was performed using the R package Sleuth (137). The likelihood ratio test and Wald test were used to identify the differentially expressed genes (the false-discovery rate-adjusted *P* value [*Q* value] was <0.05 in both tests). Since the likelihood ratio test does not produce any metric equivalent to the fold change, we used the Wald test to generate the beta statistic, which approximates to the $\log_2$ fold change in expression between the two conditions.

ChIP. ChIP-qPCR experiments on Brn1 and Scc2/Scc4 were performed as previously described (20, 35). In brief, yeast cells of a strain of interest were inoculated and grown overnight in 300 ml of YPD medium to an optical density (OD) of 1 to 2. These cells were then fixed in 1% formaldehyde for a duration of 2 h at room temperature. The reaction was then quenched with glycine, and the cells were spun down and washed in 1× PBS. The cross-linked cells were then flash frozen in dry ice and stored at −70°C. In preparation for immunoprecipitation (IP), the cells were thawed on ice, broken apart by bead beating, and sonicated to achieve a desired chromatin size of ~300 bp. Once the size of the chromatin was checked, cell debris was cleared from the sample by high-speed centrifugation. The cross-linked, sized chromatin was split into 2 samples, and IPs were done overnight in the presence of both an antibody to the protein of interest and preblocked A/G-Sepharose beads at 4°C; 50 μl of input chromatin was also taken from each IP sample prior to addition of the antibody. Chromatin elution was done using 10% Chelex 100 (Bio-Rad), along with proteinase K treatment. After elution, both input and IP DNAs were quantitated via a PicoGreen fluorescent quantification assay (Invitrogen). For each qPCR, input DNA was run in triplicate and IP DNA was run in duplicate. Equal amounts of input and IP DNAs were used in each individual reaction. The enrichment for a given probe was then calculated as IP divided by input and was further normalized to the *OCA4* locus. The results of each ChIP-qPCR were comprised of two independent cross-links for each strain assayed, and for each cross-link, two independent IPs were done.

TABLE 3 Strains and genotypes

Strain	Genotype[a]
JKY562	*MAT***a** t0Δ t1Δ t2Δ t3Δ t4Δ t5Δ t6Δ t7Δ t8Δ+t9Δ T1+T7::*HIS3* LacI-GFP::*ADE2 LEU2 BRN1*-HA::KanMx
JKY702	*MAT***a** t0Δ t1Δ t2Δ t3Δ t4Δ t5Δ t6Δ t7Δ t8Δ+t9Δ T1+T7::*HIS3 Mcd1*-13×Myc::KanMx LacI-GFP::*ADE2*
ROY5151	*MAT***a** t0Δ t1Δ t2Δ t3Δ t4Δ t5Δ t6Δ t7Δ t8Δ+t9Δ::*LEU2* T1+T7::*HIS3 ade2-1 LYS2 SCC2*-13×Myc::KanMx
ROY4825	*MAT***a** *HMR*(*s288c*) *SCC2*-13×Myc::KanMx *ADE2 his3 leu2 lys2 trp1 ura3*
ROY4925	*MAT***a** *HMR*(*s288c*) *Mcd1*-13×Myc::KanMx *ADE2*
ROY4927	*MATα HMR*(*s288c*) *BRN1*-HA::KanMx *ADE*
ROY5750	*MAT***a** LacI-GFP::*ADE2 lys2*$^-$ TEL3L::LacO::*TRP1 SPC29*-RFP::*Hyg* t0Δ t1Δ t2Δ t3Δ t4Δ t5Δ t6Δ t7Δ t8Δ+t9Δ::*LEU2?* T1+T7::*HIS3*
ROY5751	*MAT***a** LacI-GFP::*ADE2 lys2*$^-$ TEL3L::LacO::*TRP1 SPC29*-RFP::*Hyg* t0Δ t1Δ t2Δ t3Δ t4Δ t5Δ t6Δ t7Δ t8Δ+t9Δ::*LEU2?* T1+T7::*HIS3*
ROY5670	LacI-GFP::*ADE2* TEL3L::LacO::*TRP1 SPC29*-RFP::*Hyg*
ROY5671	LacI-GFP::*ADE2* TEL3L::LacO::*TRP1 SPC29*-RFP::*Hyg*
ROY5695	LacI-GFP::*ADE2 lys2*$^-$ *SRO9*::LacO::*TRP1 SPC29*-RFP::*Hyg* t0Δ t1Δ t2Δ t3Δ t4Δ t5Δ t6Δ t7Δ t8Δ+t9Δ::*LEU2* T1+T7::*HIS3*
ROY5696	LacI-GFP::*ADE2 lys2*$^-$ *SRO9*::LacO::*TRP1 SPC29*-RFP::*Hyg* t0Δ t1Δ t2Δ t3Δ t4Δ t5Δ t6Δ t7Δ t8Δ+t9Δ::*LEU2* T1+T7::*HIS3*
ROY5672	LacI-GFP::*ADE2 SRO9*::LacO::*TRP1 SPC29*-RFP::*Hyg*
ROY5689	LacI-GFP::*ADE2* 56×LacO::*LEU2 SPC29*-RFP::*Hyg* t0Δ t1Δ t2Δ t3Δ t4Δ t5Δ t6Δ t7Δ t8Δ+t9Δ T1+T7::*HIS3*
ROY5690	LacI-GFP::*ADE2* 56×LacO::*LEU2 SPC29*-RFP::*Hyg* t0Δ t1Δ t2Δ t3Δ t4Δ t5Δ t6Δ t7Δ t8Δ+t9Δ T1+T7::*HIS3*
ROY5317	*MATα* LacI-GFP::*ADE2 lys2* 56×LacO::*LEU2 SPC29*-RFP::*Hyg*
ROY5318	*MATα* LacI-GFP::*ADE2 lys2* 56×LacO::*LEU2 SPC29*-RFP::*Hyg*
ROY5290	*MATα* LacI-GFP::*ADE2* 126×LacO::*CEN3*::*TRP1 spc29*-RFP::*Hyg* t0Δ t1Δ t2Δ t3Δ t4Δ t5Δ t6Δ t7Δ t8Δ+t9Δ T1+T7::*HIS3 leu2*$^-$
ROY5291	*MATα* LacI-GFP::*ADE2* 64×LacO::*CEN3*::*TRP1 spc29*-RFP::*Hyg* t0Δ t1Δ t2Δ t3Δ t4Δ t5Δ t6Δ t7Δ t8Δ+t9Δ T1+T7::*HIS3 leu2*$^-$
ROY5288	*MAT***a** LacI-GFP::*ADE2* 126×LacO::*CEN3*::*TRP1 spc29*-RFP::*Hyg*
ROY5289	*MAT***a** LacI-GFP::*ADE2* 126×LacO::*CEN3*::*TRP1 spc29*-RFP::*Hyg*
ROY5748	*MAT***a** LacI-GFP::*ADE2* t2::56×LacO::*LEU2 SPC29*-RFP::*Hyg* t0Δ t1Δ t2Δ t3Δ t4Δ t5Δ t6Δ t7Δ t8Δ+t9Δ T1+T7::*HIS3 leu2*$^-$
ROY5749	*MAT***a** LacI-GFP::*ADE2* t2::56×LacO::*LEU2 SPC29*-RFP::*Hyg* t0Δ t1Δ t2Δ t3Δ t4Δ t5Δ t6Δ t7Δ t8Δ+t9Δ T1+T7::*HIS3 leu2*$^-$
ROY5668	*MATα* LacI-GFP::*ADE2* t2WT::56×LacO::*LEU2 SPC29*-RFP::*Hyg*
ROY5669	*MATα* LacI-GFP::*ADE2* t2WT::56×LacO::*LEU2 SPC29*-RFP::*Hyg*
ROY5319	*MAT***a** LacI-GFP::*ADE2 lys2 MAT*::LacO::*TRP1 SPC29*-RFP::*Hyg* t0Δ t1Δ t2Δ t3Δ t4Δ t5Δ t6Δ t7Δ t8Δ+t9Δ::*LEU2* T1+T7::*HIS3*
ROY5320	*MAT***a** LacI-GFP::*ADE2 lys2 MAT*::LacO::*TRP1 SPC29*-RFP::*Hyg* t0Δ t1Δ t2Δ t3Δ t4Δ t5Δ t6Δ t7Δ t8Δ+t9Δ::*LEU2* T1+T7::*HIS3*
ROY5294	*MATα* LacI-GFP::*ADE2 MAT*::LacO::*TRP1 lys2 SPC29*-RFP::*Hyg*
ROY5359	*MATα* LacI-GFP::*ADE2 lys2 MAT*::LacO::*TRP1 SPC29*-RFP::*Hyg*
ROY5687	*MAT***a** LacI-GFP::*ADE2* t1::56×LacO::*LEU2 SPC29*-RFP::*Hyg* t0Δ t1Δ t2Δ t3Δ t4Δ t5Δ t6Δ t7Δ t8Δ+t9Δ T1+T7::*HIS3 leu2*$^-$
ROY5688	*MATα* LacI-GFP::*ADE2* t1::56×LacO::*LEU2 SPC29*-RFP::*Hyg* t0Δ t1Δ t2Δ t3Δ t4Δ t5Δ t6Δ t7Δ t8Δ+t9Δ T1+T7::*HIS3 leu2*$^-$
ROY5666	*MATα* LacI-GFP::*ADE2* t1WT::56×LacO::*LEU2 SPC29*-RFP::*Hyg*
ROY5667	*MATα* LacI-GFP::*ADE2* t1WT::56×LacO::*LEU2 SPC29*-RFP::*Hyg*
ROY5321	*MATα* LacI-GFP::*ADE2 lys2 GIT1*::56×LacO::*TRP1 SPC29*-RFP::*Hyg* t0Δ t1Δ t2Δ t3Δ t4Δ t5Δ t6Δ t7Δ t8Δ+t9Δ::*LEU2* T1+T7::*HIS3*
ROY5323	*MATα* LacI-GFP::*ADE2 lys2 GIT1*::56×LacO::*TRP1 SPC29*-RFP::*Hyg* t0Δ t1Δ t2Δ t3Δ t4Δ t5Δ t6Δ t7Δ t8Δ+t9Δ::*LEU2* T1+T7::*HIS3*
ROY5664	LacI-GFP::*ADE2 GIT1*::56×LacO::*TRP1 SPC29*-RFP::*Hyg*
ROY5665	LacI-GFP::*ADE2 GIT1*::56×LacO::*TRP1 SPC29*-RFP::*Hyg*
JKY689	*MAT***a** tDNA0 (WT) t0Δ t1Δ t2Δ t3Δ t4Δ t5Δ t6Δ t7Δ t8Δ+t9Δ T1+T7::*HIS3 LEU2 ade2-1*
ROY1681	*MATα ADE2 his3 leu2 lys2 trp1 ura3 HMR* (t0Δ)
JKY690	*MAT***a** t0Δ t1Δ t2Δ t3Δ t4Δ t5Δ t6Δ t7Δ t8Δ+t9Δ T1+T7::*HIS3 LEU2 ade2-1 LYS*
JRY2334	*MAT***a** *ade2-1 can1-100 his3-11 leu2-3112 trp1-1 ura3-1 GAL*
ROY4830	*MAT***a**/*MATα HML*-TetO::*LEU2 HMR*-LacO::*TRP1* CFP-LacI-TetR-YFP::*ADE2 LYS2*
ROY4846	*MATα* 256×LacO::*GIT1*::*TRP1 HML*-TetO::*LEU2* CFP-LacI-TetR-YFP::*ADE2 tT*(*AGU*)*C*Δ::*URA3 lys2*Δ
ROY4859	*MAT HML-tetO*::*LEU2 HMR*-LacO::*TRP1* CFP-LacI-TetR-YFP::*ADE2 sir4*Δ::*URA3 lys2*
ROY4860	*MAT HML-tetO*::*LEU2 HMR*-LacO::*TRP1* CFP-LacI-TetR-YFP::*ADE2 sir4*Δ::*URA3 lys2*
ROY5518	*MAT***a** LacI-GFP::*ADE2 lys2 SRO9*::LacO::*TRP1* t0Δ t1Δ t2Δ t3Δ t4Δ t5Δ t6Δ t7Δ t8Δ+t9Δ::*LEU2* T1+T7::*HIS3*
ROY5521	*MAT***a** *lys*$^-$ LacI-GFP::*ADE2 SRO9*::LacO::*TRP1*
ROY5602	*MAT***a** LacI-GFP::*ADE2* 56×LacO::*LEU2* t0Δ t1Δ t2Δ t3Δ t4Δ t5Δ t6Δ t7Δ t8Δ+t9Δ T1+T7::*HIS3*
GRY911	*MAT***a** LacI-GFP::*ADE2* 56×LacO::*LEU2 lys2*
GRY907	*MATα* LacI-GFP::*ADE2* 56×LacO::*LEU2 lys2 trp1 ura3 his3*
GRY872	*MATα* 126×LacO::*CEN3*::*TRP1* t0Δ t1Δ t2Δ t3Δ t4Δ t5Δ t6Δ t7Δ t8Δ+t9Δ T1+T7::*HIS3 leu2-3112* LacI-GFP::*ADE2 trp1 lys2 ura3*
GRY823	*MAT***a** LacI-GFP::*ADE2* 64×LacO::*CEN3*::*TRP1*
GRY824	*MATα* LacI-GFP::*ADE2* 64×LacO::*CEN3*::*TRP1*
ROY5512	*MAT***a** LacI-GFP::*ADE2* t2::56×LacO::*LEU2* t0Δ t1Δ t2Δ t3Δ t4Δ t5Δ t6Δ t7Δ t8Δ+t9Δ T1+T7::*HIS3 leu2*
ROY5510	*MATα lys*$^-$ LacI-GFP::*ADE2* t2WT::56×LacO::*LEU2*
GRY938	*MATα* t1Δ::*URA3* t0Δ t1Δ t2Δ t3Δ t4Δ t5Δ t6Δ t7Δ t8Δ+t9Δ::*LEU2* T1+T7::*HIS3* LacI-GFP::*ADE2 HMR-GIT1*::*TRP1 lys*
GRY883	*MATα* t1WT*αHIS3* t1WT::*URA3 GIT1*::*TRP1 LYS*$^+$ *LEU*$^+$ *ade2*
GRY935	*MAT***a** LacI-GFP::*ADE2* t0Δ t1Δ t2Δ t3Δ t4Δ t5Δ t6Δ t7Δ t8Δ+t9Δ T1+T7::*HIS3 trp1 leu2 lys2 ura3*
GRY963	*MATα* t0Δ t1Δ t2Δ t3Δ t4Δ t5Δ t6Δ t7Δ t8Δ+t9Δ T1+T7::*HIS3 LYS*$^+$ *ade2 leu2*
JRY4012	*MAT***a** *can1-100 his3-11 leu2-3112 lys2*Δ *trp1-1 ura3-1 GAL*

[a]t8Δ+T9Δ indicates that the two genes were deleted simultaneously. T1+T7 indicates that the two genes were inserted adjacent to one another.

Mean squared distance analysis. Mean squared distance (MSD) analysis was carried out as previously described (68, 138, 139). In brief, we built strains that contained a 64×LacO array at specific points along chromosome III. We then integrated a cassette containing an spc29-RFP fusion protein elsewhere in the genome. This protein is an essential kinetochore protein and therefore serves as a

TABLE 4 Sequences of PCR primers used in this study

Primer name	Sequence (5′–3′)	Amplicon
yOH58	TACTACAAGAGAAAGGCCATCTCC	t1
yOH59	AATGCAGCGCAGACAGCACAGTT	t1
QJK61	TTGAGATACAAAATATTACAAGAAGTCCTG	t2
QJK62	GCGTTCTTCTGTATCTGAAGATAGTG	t2
QJK63	TCATGTATCAAGATTACTAGCGCAAGTG	t5
QJK64	TTCTATTCTTATGTACCGTTCCGCC	t5
yOH62	GCAAGCGAAGTTGTTCCCGTTAT	t7
yOH63	GTTCGGTCACTTAGAGGATATAATTG	t7
QJK69	CTCTATTTCTCAACAAGTAATTGGTTGTTT	t8
QJK70	GCCCCTGTGTGTTCTCGTTATGT	t8
yOH64	GACAAGAAAGATAACGACACAGTGA	t9
yOH65	GGCCCTCGTATAGTCTCTTTTC	t9
R197	GAGACCAGGTTTATTCAACCGGTAAC	t0
LOU120	GGGTGTCACCGAATAACGTGAT	t0
GRO39	TAAGACAATTGTGGACAACAAAGCAAA	*OCA4*
GRO40	ATTTATTAATGTCAAAAGCCGCTGAGG	*OCA4*
yOH66	TCACTCATATAAACCGAACCCTTCC	CEN3
yOH67	GGATTTTCCATATTGTTTGGCGCTG	CEN3

marker for the spindle pole body. The spindle pole body served as a fixed point at which we could measure the movement of our GFP-tagged loci in 3D space over a period of 10 min. Z-stack images of the cells were taken every 30 s during the time-lapse movie, and the data were used to calculate the radius of constraint using the following formula: MSD $= (X_{t+T} - X_t)^2 + (Y_{t+T} - Y_t)^2$, where X and Y are the coordinates of the fluorescent dot, T is the time lag, and t is the time. MSD curves were generated for each locus in both the WT and tDNA delete strains. The MSD curves were used to calculate the Rc for each locus. The analysis was performed in no less than 35 cells per genotype assayed. The data were plotted in NotBoxPlots (the source code was obtained from https://github.com/raacampbell/notBoxPlot).

***HML-HMR* colocalization analysis.** Distance assays between *HML* and *HMR* were performed as previously described (20). Fluorescence microscopy was performed on live yeast cells after growing the cells in yeast minimal dextrose (YMD) with leucine, uracil, tryptophan, lysine, adenine, and histidine. The cells were grown to an A_{600} of approximately 0.6. The cells were washed in YMD, placed on YMD-agar patches on slides, and imaged. Microscopy was performed with an Olympus xi70 inverted wide-field microscope with a DeltaVision precision stage using a Coolsnap HQ2 camera and a 100×/1.4-numerical-aperture oil objective. The 20 image stacks for each image were acquired with a step size of 200 nm using the appropriate wavelength for CFP, YFP, GFP, or mCherry. The acquisition software used was softWoRx3.7.1. The images were cropped using Adobe Photoshop. For the distance analysis between *HML* and *HMR*, the distances between the yellow and cyan dots were calculated in nanometers using the "measure" tool in three dimensions. The measured distances were loaded into R software (www.r-project.org), and the data were plotted as a box plot. The box included the middle 50% of the data, with the line in the box indicating the median value. The data presented are the sums of at least two independent strains.

Single-cell expression analysis. Single-cell expression analysis was performed as previously described (93). Briefly, cells were grown in YPD at 30°C and placed in a microfluidics device. Time-lapse photographs of growing cells were recorded using an Axio Observer Z1 microscope with a 40× objective. The ECYP and EYFP fluorescence intensities were normalized to the highest level of fluorescence observed and to the euchromatic mCherry signal.

Micro-C. Micro-C was performed as previously described (71). The detailed method has been described previously (72). In brief, the technique provides nucleosome level resolution of all of the interactions occurring across the genome by using MNase digestion in lieu of a restriction enzyme, as in traditional Hi-C techniques.

Antibodies. The antibodies used in ChIP were as follows: Scc2-Myc, anti-myc 9E10 (Abcam; 5 μl); Brn1-HA, anti-HA HA.11 (Covance; 5 μl).

Accession number(s). The interactome data were deposited in the GEO database under accession no. GSE98543. The MNase-seq data are available in the GEO database under accession no. GSE98304. CHIP-seq and RNA-seq data have been deposited in the GEO database under accession no. GSE106250.

ACKNOWLEDGMENTS

This work was supported in part by a grant from the NIH to R.T.K. (GM078068) and T32-GM008646 to J.G.K., O.H., and K.Y.W. This study was funded in part by the Intramural Research Program of the National Institutes of Health (NICHD).

We thank the NHLBI Core Facility for paired-end sequencing of the micrococcal nuclease libraries. The Functional Genomics Laboratory, UC Berkeley, sequenced the ChIP-seq libraries on an Illumina HiSeq 4000 at the Vincent J. Coates Laboratory at UC Berkeley, supported by an NIH S10 OD018174 Instrumentation Grant.

REFERENCES

1. Taddei A, Schober H, Gasser SM. 2010. The budding yeast nucleus. Cold Spring Harb Perspect Biol 2:a000612. https://doi.org/10.1101/cshperspect.a000612.
2. Zimmer C, Fabre E. 2011. Principles of chromosomal organization: lessons from yeast. J Cell Biol 192:723–733. https://doi.org/10.1083/jcb.201010058.
3. Palladino F, Laroche T, Gilson E, Pillus L, Gasser SM. 1993. The positioning of yeast telomeres depends on SIR3, SIR4, and the integrity of the nuclear membrane. Cold Spring Harbor Symp Quant Biol 58:733–746. https://doi.org/10.1101/SQB.1993.058.01.081.
4. Ruben GJ, Kirkland JG, Macdonough T, Chen M, Dubey RN, Gartenberg MR, Kamakaka RT. 2011. Nucleoporin mediated nuclear positioning and silencing of HMR. PLoS One 6:e21923. https://doi.org/10.1371/journal.pone.0021923.
5. Fabre E, Spichal M. 2014. Subnuclear architecture of telomeres and subtelomeres in yeast, p 13–37. *In* Louis EJ, Becker MM (ed), SubTelomeres. Springer, New York, NY.
6. Oakes M, Aris JP, Brockenbrough JS, Wai H, Vu L, Nomura M. 1998. Mutational analysis of the structure and localization of the nucleolus in the yeast *Saccharomyces cerevisiae*. J Cell Biol 143:23–34. https://doi.org/10.1083/jcb.143.1.23.
7. Jin QW, Fuchs J, Loidl J. 2000. Centromere clustering is a major determinant of yeast interphase nuclear organization. J Cell Sci 113:1903–1912.
8. Therizols P, Duong T, Dujon B, Zimmer C, Fabre E. 2010. Chromosome arm length and nuclear constraints determine the dynamic relationship of yeast subtelomeres. Proc Natl Acad Sci U S A 107:2025–2030. https://doi.org/10.1073/pnas.0914187107.
9. Tjong H, Gong K, Chen L, Alber F. 2012. Physical tethering and volume exclusion determine higher-order genome organization in budding yeast. Genome Res 22:1295–1305. https://doi.org/10.1101/gr.129437.111.
10. Duan Z, Andronescu M, Schutz K, McIlwain S, Kim YJ, Lee C, Shendure J, Fields S, Blau CA, Noble WS. 2010. A three-dimensional model of the yeast genome. Nature 465:363–367. https://doi.org/10.1038/nature08973.
11. Palladino F, Laroche T, Gilson E, Axelrod A, Pillus L, Gasser SM. 1993. SIR3 and SIR4 proteins are required for the positioning and integrity of yeast telomeres. Cell 75:543–555. https://doi.org/10.1016/0092-8674(93)90388-7.
12. Andrulis ED, Zappulla DC, Ansari A, Perrod S, Laiosa CV, Gartenberg MR, Sternglanz R. 2002. Esc1, a nuclear periphery protein required for Sir4-based plasmid anchoring and partitioning. Mol Cell Biol 22:8292–8301. https://doi.org/10.1128/MCB.22.23.8292-8301.2002.
13. Taddei A, Hediger F, Neumann FR, Bauer C, Gasser SM. 2004. Separation of silencing from perinuclear anchoring functions in yeast Ku80, Sir4 and Esc1 proteins. EMBO J 23:1301–1312. https://doi.org/10.1038/sj.emboj.7600144.
14. Taddei A, Gartenberg MR, Neumann FR, Hediger F, Gasser SM. 2005. Multiple pathways tether telomeres and silent chromatin at the nuclear periphery: functional implications for sir-mediated repression. Novartis Found Symp 264:140–156.
15. Bupp JM, Martin AE, Stensrud ES, Jaspersen SL. 2007. Telomere anchoring at the nuclear periphery requires the budding yeast Sad1-UNC-84 domain protein Mps3. J Cell Biol 179:845–854. https://doi.org/10.1083/jcb.200706040.
16. Mekhail K, Seebacher J, Gygi SP, Moazed D. 2008. Role for perinuclear chromosome tethering in maintenance of genome stability. Nature 456:667–670. https://doi.org/10.1038/nature07460.
17. Klein F, Laroche T, Cardenas ME, Hofmann JF, Schweizer D, Gasser SM. 1992. Localization of RAP1 and topoisomerase II in nuclei and meiotic chromosomes of yeast. J Cell Biol 117:935–948. https://doi.org/10.1083/jcb.117.5.935.
18. Taddei A, Van Houwe G, Hediger F, Kalck V, Cubizolles F, Schober H, Gasser SM. 2006. Nuclear pore association confers optimal expression levels for an inducible yeast gene. Nature 441:774–778. https://doi.org/10.1038/nature04845.
19. Kirkland J, Peterson MR, Still CB, Brueggemman L, Dhillon N, Kamakaka R. 2015. Heterochromatin formation via recruitment of DNA repair proteins. Mol Biol Cell 26:1395–1410. https://doi.org/10.1091/mbc.E14-09-1413.
20. Kirkland JG, Kamakaka RT. 2013. Long-range heterochromatin association is mediated by silencing and double-strand DNA break repair proteins. J Cell Biol 201:809–826. https://doi.org/10.1083/jcb.201211105.
21. Dieci G, Fiorino G, Castelnuovo M, Teichmann M, Pagano A. 2007. The expanding RNA polymerase III transcriptome. Trends Genet 23:614–622. https://doi.org/10.1016/j.tig.2007.09.001.
22. Oki M, Kamakaka RT. 2005. Barrier function at HMR. Mol Cell 19:707–716. https://doi.org/10.1016/j.molcel.2005.07.022.
23. Weiner A, Hughes A, Yassour M, Rando OJ, Friedman N. 2010. High-resolution nucleosome mapping reveals transcription-dependent promoter packaging. Genome Res 20:90–100. https://doi.org/10.1101/gr.098509.109.
24. Yuan GC, Liu YJ, Dion MF, Slack MD, Wu LF, Altschuler SJ, Rando OJ. 2005. Genome-scale identification of nucleosome positions in *S. cerevisiae*. Science 309:626–630. https://doi.org/10.1126/science.1112178.
25. Cole HA, Howard BH, Clark DJ. 2012. Genome-wide mapping of nucleosomes in yeast using paired-end sequencing. Methods Enzymol 513:145–168. https://doi.org/10.1016/B978-0-12-391938-0.00006-9.
26. Geiduschek EP, Kassavetis GA. 2001. The RNA polymerase III transcription apparatus. J Mol Biol 310:1–26. https://doi.org/10.1006/jmbi.2001.4732.
27. Schramm L, Hernandez N. 2002. Recruitment of RNA polymerase III to its target promoters. Genes Dev 16:2593–2620. https://doi.org/10.1101/gad.1018902.
28. Glynn EF, Megee PC, Yu HG, Mistrot C, Unal E, Koshland DE, DeRisi JL, Gerton JL. 2004. Genome-wide mapping of the cohesin complex in the yeast *Saccharomyces cerevisiae*. PLoS Biol 2:E259. https://doi.org/10.1371/journal.pbio.0020259.
29. D'Ambrosio C, Schmidt CK, Katou Y, Kelly G, Itoh T, Shirahige K, Uhlmann F. 2008. Identification of *cis*-acting sites for condensin loading onto budding yeast chromosomes. Genes Dev 22:2215–2227. https://doi.org/10.1101/gad.1675708.
30. Haeusler RA, Pratt-Hyatt M, Good PD, Gipson TA, Engelke DR. 2008. Clustering of yeast tRNA genes is mediated by specific association of condensin with tRNA gene transcription complexes. Genes Dev 22:2204–2214. https://doi.org/10.1101/gad.1675908.
31. Lopez-Serra L, Kelly G, Patel H, Stewart A, Uhlmann F. 2014. The Scc2-Scc4 complex acts in sister chromatid cohesion and transcriptional regulation by maintaining nucleosome-free regions. Nat Genet 46:1147–1151. https://doi.org/10.1038/ng.3080.
32. Kogut I, Wang J, Guacci V, Mistry RK, Megee PC. 2009. The Scc2/Scc4 cohesin loader determines the distribution of cohesin on budding yeast chromosomes. Genes Dev 23:2345–2357. https://doi.org/10.1101/gad.1819409.
33. Bausch C, Noone S, Henry JM, Gaudenz K, Sanderson B, Seidel C, Gerton JL. 2007. Transcription alters chromosomal locations of cohesin in *Saccharomyces cerevisiae*. Mol Cell Biol 27:8522–8532. https://doi.org/10.1128/MCB.01007-07.
34. Huang J, Laurent BC. 2004. A role for the RSC chromatin remodeler in regulating cohesion of sister chromatid arms. Cell Cycle 3:973–975.
35. Dhillon N, Raab J, Guzzo J, Szyjka SJ, Gangadharan S, Aparicio OM, Andrews B, Kamakaka RT. 2009. DNA polymerase epsilon, acetylases and remodellers cooperate to form a specialized chromatin structure at a tRNA insulator. EMBO J 28:2583–2600. https://doi.org/10.1038/emboj.2009.198.
36. Frenkel FE, Chaley MB, Korotkov EV, Skryabin KG. 2004. Evolution of tRNA-like sequences and genome variability. Gene 335:57–71. https://doi.org/10.1016/j.gene.2004.03.005.
37. Goodenbour JM, Pan T. 2006. Diversity of tRNA genes in eukaryotes. Nucleic Acids Res 34:6137–6146. https://doi.org/10.1093/nar/gkl725.
38. Withers M, Wernisch L, dos Reis M. 2006. Archaeology and evolution of transfer RNA genes in the *Escherichia coli* genome. RNA 12:933–942. https://doi.org/10.1261/rna.2272306.
39. Raab JR, Chiu J, Zhu J, Katzman S, Kurukuti S, Wade PA, Haussler D, Kamakaka RT. 2012. Human tRNA genes function as chromatin insulators. EMBO J 31:330–350. https://doi.org/10.1038/emboj.2011.406.
40. Wang J, Lunyak VV, Jordan IK. 2012. Genome-wide prediction and analysis of human chromatin boundary elements. Nucleic Acids Res 40:511–529. https://doi.org/10.1093/nar/gkr750.
41. Van Bortle K, Corces VG. 2012. tDNA insulators and the emerging role of TFIIIC in genome organization. Transcription 3:277–284. https://doi.org/10.4161/trns.21579.

42. Kirkland JG, Raab JR, Kamakaka RT. 2013. TFIIIC bound DNA elements in nuclear organization and insulation. Biochim Biophys Acta 1829: 418–424. https://doi.org/10.1016/j.bbagrm.2012.09.006.
43. Donze D, Adams CR, Rine J, Kamakaka RT. 1999. The boundaries of the silenced HMR domain in *Saccharomyces cerevisiae*. Genes Dev 13: 698–708. https://doi.org/10.1101/gad.13.6.698.
44. Biswas M, Maqani N, Rai R, Kumaran SP, Iyer KR, Sendinc E, Smith JS, Laloraya S. 2009. Limiting the extent of the RDN1 heterochromatin domain by a silencing barrier and Sir2 protein levels in *Saccharomyces cerevisiae*. Mol Cell Biol 29:2889–2898. https://doi.org/10.1128/MCB.00728-08.
45. Korde A, Rosselot JM, Donze D. 2014. Intergenic transcriptional interference is blocked by RNA polymerase III transcription factor TFIIIB in *Saccharomyces cerevisiae*. Genetics 196:427–438. https://doi.org/10.1534/genetics.113.160093.
46. Simms TA, Miller EC, Buisson NP, Jambunathan N, Donze D. 2004. The *Saccharomyces cerevisiae* TRT2 tRNAThr gene upstream of STE6 is a barrier to repression in MATalpha cells and exerts a potential tRNA position effect in MATa cells. Nucleic Acids Res 32:5206–5213. https://doi.org/10.1093/nar/gkh858.
47. Simms TA, Dugas SL, Gremillion JC, Ibos ME, Dandurand MN, Toliver TT, Edwards DJ, Donze D. 2008. TFIIIC binding sites function as both heterochromatin barriers and chromatin insulators in *Saccharomyces cerevisiae*. Eukaryot Cell 7:2078–2086. https://doi.org/10.1128/EC.00128-08.
48. Van Bortle K, Nichols MH, Li L, Ong CT, Takenaka N, Qin ZS, Corces VG. 2014. Insulator function and topological domain border strength scale with architectural protein occupancy. Genome Biol 15:R82. https://doi.org/10.1186/gb-2014-15-5-r82.
49. Ebersole T, Kim JH, Samoshkin A, Kouprina N, Pavlicek A, White RJ, Larionov V. 2011. tRNA genes protect a reporter gene from epigenetic silencing in mouse cells. Cell Cycle 10:2779–2791. https://doi.org/10.4161/cc.10.16.17092.
50. Dixon JR, Selvaraj S, Yue F, Kim A, Li Y, Shen Y, Hu M, Liu JS, Ren B. 2012. Topological domains in mammalian genomes identified by analysis of chromatin interactions. Nature 485:376–380. https://doi.org/10.1038/nature11082.
51. Good PD, Kendall A, Ignatz-Hoover J, Miller EL, Pai DA, Rivera SR, Carrick B, Engelke DR. 2013. Silencing near tRNA genes is nucleosome-mediated and distinct from boundary element function. Gene 526: 7–15. https://doi.org/10.1016/j.gene.2013.05.016.
52. Thompson M, Haeusler RA, Good PD, Engelke DR. 2003. Nucleolar clustering of dispersed tRNA genes. Science 302:1399–1401. https://doi.org/10.1126/science.1089814.
53. Pombo A, Jackson DA, Hollinshead M, Wang Z, Roeder RG, Cook PR. 1999. Regional specialization in human nuclei: visualization of discrete sites of transcription by RNA polymerase III. EMBO J 18:2241–2253. https://doi.org/10.1093/emboj/18.8.2241.
54. Haeusler RA, Engelke DR. 2006. Spatial organization of transcription by RNA polymerase III. Nucleic Acids Res 34:4826–4836. https://doi.org/10.1093/nar/gkl656.
55. Iwasaki O, Tanaka A, Tanizawa H, Grewal SI, Noma K. 2010. Centromeric localization of dispersed Pol III genes in fission yeast. Mol Biol Cell 21:254–265. https://doi.org/10.1091/mbc.e09-09-0790.
56. Schalbetter SA, Goloborodko A, Fudenberg G, Belton JM, Miles C, Yu M, Dekker J, Mirny L, Baxter J. 2017. SMC complexes differentially compact mitotic chromosomes according to genomic context. Nat Cell Biol 19:1071–1080. https://doi.org/10.1038/ncb3594.
57. Haeusler RA, Engelke DR. 2004. Genome organization in three dimensions: thinking outside the line. Cell Cycle 3:273–275.
58. Iwasaki O, Noma K. 2012. Global genome organization mediated by RNA polymerase III-transcribed genes in fission yeast. Gene 493: 195–200. https://doi.org/10.1016/j.gene.2010.12.011.
59. Ho CK, Abelson J. 1988. Testing for intron function in the essential Saccharomyces cerevisiae tRNA(SerUCG) gene. J Mol Biol 202:667–672. https://doi.org/10.1016/0022-2836(88)90295-1.
60. Bloom-Ackermann Z, Navon S, Gingold H, Towers R, Pilpel Y, Dahan O. 2014. A comprehensive tRNA deletion library unravels the genetic architecture of the tRNA pool. PLoS Genet 10:e1004084. https://doi.org/10.1371/journal.pgen.1004084.
61. Dion MF, Kaplan T, Kim M, Buratowski S, Friedman N, Rando OJ. 2007. Dynamics of replication-independent histone turnover in budding yeast. Science 315:1405–1408. https://doi.org/10.1126/science.1134053.
62. Chereji RV, Ocampo J, Clark DJ. 2017. MNase-sensitive complexes in yeast: nucleosomes and non-histone barriers. Mol Cell 65:565–577 e3. https://doi.org/10.1016/j.molcel.2016.12.009.
63. Uhlmann F. 2016. SMC complexes: from DNA to chromosomes. Nat Rev Mol Cell Biol 17:399–412. https://doi.org/10.1038/nrm.2016.30.
64. Parnell TJ, Huff JT, Cairns BR. 2008. RSC regulates nucleosome positioning at Pol II genes and density at Pol III genes. EMBO J 27:100–110. https://doi.org/10.1038/sj.emboj.7601946.
65. Damelin M, Simon I, Moy TI, Wilson B, Komili S, Tempst P, Roth FP, Young RA, Cairns BR, Silver PA. 2002. The genome-wide localization of Rsc9, a component of the RSC chromatin-remodeling complex, changes in response to stress. Mol Cell 9:563–573. https://doi.org/10.1016/S1097-2765(02)00475-6.
66. Dion V, Kalck V, Horigome C, Towbin BD, Gasser SM. 2012. Increased mobility of double-strand breaks requires Mec1, Rad9 and the homologous recombination machinery. Nat Cell Biol 14:502–509. https://doi.org/10.1038/ncb2465.
67. Mine-Hattab J, Rothstein R. 2012. Increased chromosome mobility facilitates homology search during recombination. Nat Cell Biol 14: 510–517. https://doi.org/10.1038/ncb2472.
68. Verdaasdonk JS, Vasquez PA, Barry RM, Barry T, Goodwin S, Forest MG, Bloom K. 2013. Centromere tethering confines chromosome domains. Mol Cell 52:819–831. https://doi.org/10.1016/j.molcel.2013.10.021.
69. Albert B, Mathon J, Shukla A, Saad H, Normand C, Leger-Silvestre I, Villa D, Kamgoue A, Mozziconacci J, Wong H, Zimmer C, Bhargava P, Bancaud A, Gadal O. 2013. Systematic characterization of the conformation and dynamics of budding yeast chromosome XII. J Cell Biol 202: 201–210. https://doi.org/10.1083/jcb.201208186.
70. Noma K, Cam HP, Maraia RJ, Grewal SI. 2006. A role for TFIIIC transcription factor complex in genome organization. Cell 125:859–872. https://doi.org/10.1016/j.cell.2006.04.028.
71. Hsieh TH, Weiner A, Lajoie B, Dekker J, Friedman N, Rando OJ. 2015. Mapping nucleosome resolution chromosome folding in yeast by micro-C. Cell 162:108–119. https://doi.org/10.1016/j.cell.2015.05.048.
72. Hsieh TS, Fudenberg G, Goloborodko A, Rando OJ. 2016. Micro-C XL: assaying chromosome conformation from the nucleosome to the entire genome. Nat Methods 13:1009–1011. https://doi.org/10.1038/nmeth.4025.
73. Guacci V, Hogan E, Koshland D. 1997. Centromere position in budding yeast: evidence for anaphase A. Mol Biol Cell 8:957–972. https://doi.org/10.1091/mbc.8.6.957.
74. Jin Q, Trelles-Sticken E, Scherthan H, Loidl J. 1998. Yeast nuclei display prominent centromere clustering that is reduced in nondividing cells and in meiotic prophase. J Cell Biol 141:21–29. https://doi.org/10.1083/jcb.141.1.21.
75. Dekker J, Rippe K, Dekker M, Kleckner N. 2002. Capturing chromosome conformation. Science 295:1306–1311. https://doi.org/10.1126/science.1067799.
76. Kumaran R, Yang SY, Leu JY. 2013. Characterization of chromosome stability in diploid, polyploid and hybrid yeast cells. PLoS One 8:e68094. https://doi.org/10.1371/journal.pone.0068094.
77. Miele A, Bystricky K, Dekker J. 2009. Yeast silent mating type loci form heterochromatic clusters through silencer protein-dependent long-range interactions. PLoS Genet 5:e1000478. https://doi.org/10.1371/journal.pgen.1000478.
78. Dubarry M, Loiodice I, Chen CL, Thermes C, Taddei A. 2011. Tight protein-DNA interactions favor gene silencing. Genes Dev 25:1365–1370. https://doi.org/10.1101/gad.611011.
79. Giorgetti L, Heard E. 2016. Closing the loop: 3C versus DNA FISH. Genome Biol 17:215. https://doi.org/10.1186/s13059-016-1081-2.
80. Fraser J, Williamson I, Bickmore WA, Dostie J. 2015. An overview of genome organization and how we got there: from FISH to Hi-C. Microbiol Mol Biol Rev 79:347–372. https://doi.org/10.1128/MMBR.00006-15.
81. Williamson I, Berlivet S, Eskeland R, Boyle S, Illingworth RS, Paquette D, Dostie J, Bickmore WA. 2014. Spatial genome organization: contrasting views from chromosome conformation capture and fluorescence in situ hybridization. Genes Dev 28:2778–2791. https://doi.org/10.1101/gad.251694.114.
82. Dubey RN, Gartenberg MR. 2007. A tDNA establishes cohesion of a neighboring silent chromatin domain. Genes Dev 21:2150–2160. https://doi.org/10.1101/gad.1583807.
83. Donze D, Kamakaka RT. 2001. RNA polymerase III and RNA polymerase II promoter complexes are heterochromatin barriers in *Saccharomyces cerevisiae*. EMBO J 20:520–531. https://doi.org/10.1093/emboj/20.3.520.

84. Valenzuela L, Dhillon N, Kamakaka RT. 2009. Transcription independent insulation at TFIIIC-dependent insulators. Genetics 183:131–148. https://doi.org/10.1534/genetics.109.106203.
85. Dilworth DJ, Tackett AJ, Rogers RS, Yi EC, Christmas RH, Smith JJ, Siegel AF, Chait BT, Wozniak RW, Aitchison JD. 2005. The mobile nucleoporin Nup2p and chromatin-bound Prp20p function in endogenous NPC-mediated transcriptional control. J Cell Biol 171:955–965. https://doi.org/10.1083/jcb.200509061.
86. Deshpande AM, Newlon CS. 1996. DNA replication fork pause sites dependent on transcription. Science 272:1030–1033. https://doi.org/10.1126/science.272.5264.1030.
87. Azvolinsky A, Giresi PG, Lieb JD, Zakian VA. 2009. Highly transcribed RNA polymerase II genes are impediments to replication fork progression in *Saccharomyces cerevisiae*. Mol Cell 34:722–734. https://doi.org/10.1016/j.molcel.2009.05.022.
88. Achar YJ, Foiani M. 2017. Coordinating replication with transcription. Adv Exp Med Biol 1042:455–487. https://doi.org/10.1007/978-981-10-6955-0_20.
89. Szilard RK, Jacques PE, Laramee L, Cheng B, Galicia S, Bataille AR, Yeung M, Mendez M, Bergeron M, Robert F, Durocher D. 2010. Systematic identification of fragile sites via genome-wide location analysis of gamma-H2AX. Nat Struct Mol Biol 17:299–305. https://doi.org/10.1038/nsmb.1754.
90. Lengronne A, Katou Y, Mori S, Yokobayashi S, Kelly GP, Itoh T, Watanabe Y, Shirahige K, Uhlmann F. 2004. Cohesin relocation from sites of chromosomal loading to places of convergent transcription. Nature 430:573–578. https://doi.org/10.1038/nature02742.
91. Ivessa AS, Lenzmeier BA, Bessler JB, Goudsouzian LK, Schnakenberg SL, Zakian VA. 2003. The *Saccharomyces cerevisiae* helicase Rrm3p facilitates replication past nonhistone protein-DNA complexes. Mol Cell 12:1525–1536. https://doi.org/10.1016/S1097-2765(03)00456-8.
92. Azvolinsky A, Dunaway S, Torres JZ, Bessler JB, Zakian VA. 2006. The *S. cerevisiae* Rrm3p DNA helicase moves with the replication fork and affects replication of all yeast chromosomes. Genes Dev 20:3104–3116. https://doi.org/10.1101/gad.1478906.
93. Mano Y, Kobayashi TJ, Nakayama J, Uchida H, Oki M. 2013. Single cell visualization of yeast gene expression shows correlation of epigenetic switching between multiple heterochromatic regions through multiple generations. PLoS Biol 11:e1001601. https://doi.org/10.1371/journal.pbio.1001601.
94. Valenzuela L, Gangadharan S, Kamakaka RT. 2006. Analyses of SUM1-1-mediated long-range repression. Genetics 172:99–112. https://doi.org/10.1534/genetics.105.050427.
95. Valenzuela L, Dhillon N, Dubey RN, Gartenberg MR, Kamakaka RT. 2008. Long-range communication between the silencers of HMR. Mol Cell Biol 28:1924–1935. https://doi.org/10.1128/MCB.01647-07.
96. Fu Y, Sinha M, Peterson CL, Weng Z. 2008. The insulator binding protein CTCF positions 20 nucleosomes around its binding sites across the human genome. PLoS Genet 4:e1000138. https://doi.org/10.1371/journal.pgen.1000138.
97. Nagarajavel V, Iben JR, Howard BH, Maraia RJ, Clark DJ. 2013. Global 'bootprinting' reveals the elastic architecture of the yeast TFIIIB-TFIIIC transcription complex in vivo. Nucleic Acids Res 41:8135–8143. https://doi.org/10.1093/nar/gkt611.
98. Roberts DN, Stewart AJ, Huff JT, Cairns BR. 2003. The RNA polymerase III transcriptome revealed by genome-wide localization and activity-occupancy relationships. Proc Natl Acad Sci U S A 100:14695–14700. https://doi.org/10.1073/pnas.2435566100.
99. Moqtaderi Z, Struhl K. 2004. Genome-wide occupancy profile of the RNA polymerase III machinery in *Saccharomyces cerevisiae* reveals loci with incomplete transcription complexes. Mol Cell Biol 24:4118–4127. https://doi.org/10.1128/MCB.24.10.4118-4127.2004.
100. Harismendy O, Gendrel CG, Soularue P, Gidrol X, Sentenac A, Werner M, Lefebvre O. 2003. Genome-wide location of yeast RNA polymerase III transcription machinery. EMBO J 22:4738–4747. https://doi.org/10.1093/emboj/cdg466.
101. Blat Y, Kleckner N. 1999. Cohesins bind to preferential sites along yeast chromosome III, with differential regulation along arms versus the centric region. Cell 98:249–259. https://doi.org/10.1016/S0092-8674(00)81019-3.
102. Laloraya S, Guacci V, Koshland D. 2000. Chromosomal addresses of the cohesin component Mcd1p. J Cell Biol 151:1047–1056. https://doi.org/10.1083/jcb.151.5.1047.
103. Lindroos HB, Strom L, Itoh T, Katou Y, Shirahige K, Sjogren C. 2006. Chromosomal association of the Smc5/6 complex reveals that it functions in differently regulated pathways. Mol Cell 22:755–767. https://doi.org/10.1016/j.molcel.2006.05.014.
104. Klein F, Mahr P, Galova M, Buonomo SB, Michaelis C, Nairz K, Nasmyth K. 1999. A central role for cohesins in sister chromatid cohesion, formation of axial elements, and recombination during yeast meiosis. Cell 98:91–103. https://doi.org/10.1016/S0092-8674(00)80609-1.
105. Noma KI. 2017. The yeast genomes in three dimensions: mechanisms and functions. Annu Rev Genet 51:23–44. https://doi.org/10.1146/annurev-genet-120116-023438.
106. Heidinger-Pauli JM, Mert O, Davenport C, Guacci V, Koshland D. 2010. Systematic reduction of cohesin differentially affects chromosome segregation, condensation, and DNA repair. Curr Biol 20:957–963. https://doi.org/10.1016/j.cub.2010.04.018.
107. Annaluru N, Muller H, Mitchell LA, Ramalingam S, Stracquadanio G, Richardson SM, Dymond JS, Kuang Z, Scheifele LZ, Cooper EM, Cai Y, Zeller K, Agmon N, Han JS, Hadjithomas M, Tullman J, Caravelli K, Cirelli K, Guo Z, London V, Yeluru A, Murugan S, Kandavelou K, Agier N, Fischer G, Yang K, Martin JA, Bilgel M, Bohutskyi P, Boulier KM, Capaldo BJ, Chang J, Charoen K, Choi WJ, Deng P, DiCarlo JE, Doong J, Dunn J, Feinberg JI, Fernandez C, Floria CE, Gladowski D, Hadidi P, Ishizuka I, Jabbari J, Lau CYL, Lee PA, Li S, Lin D, Linder ME, Ling J, Liu J, Liu J, London M, Ma H, Mao J, McDade JE, McMillan A, Moore AM, Oh WC, Ouyang Y, Patel R, Paul M, Paulsen LC, Qiu J, Rhee A, Rubashkin MG, Soh IY, Sotuyo NE, Srinivas V, Suarez A, Wong A, Wong R, Xie WR, Xu Y, Yu AT, Koszul R, Bader JS, Boeke JD, Chandrasegaran S. 2014. Total synthesis of a functional designer eukaryotic chromosome. Science 344:55–58. https://doi.org/10.1126/science.1249252.
108. Mercy G, Mozziconacci J, Scolari VF, Yang K, Zhao G, Thierry A, Luo Y, Mitchell LA, Shen M, Shen Y, Walker R, Zhang W, Wu Y, Xie ZX, Luo Z, Cai Y, Dai J, Yang H, Yuan YJ, Boeke JD, Bader JS, Muller H, Koszul R. 2017. 3D organization of synthetic and scrambled chromosomes. Science 355:eaaf4597. https://doi.org/10.1126/science.aaf4597.
109. Dujon B. 1996. The yeast genome project: what did we learn? Trends Genet 12:263–270. https://doi.org/10.1016/0168-9525(96)10027-5.
110. Sharp PM, Lloyd AT. 1993. Regional base composition variation along yeast chromosome III: evolution of chromosome primary structure. Nucleic Acids Res 21:179–183. https://doi.org/10.1093/nar/21.2.179.
111. Dekker J. 2007. GC- and AT-rich chromatin domains differ in conformation and histone modification status and are differentially modulated by Rpd3p. Genome Biol 8:R116. https://doi.org/10.1186/gb-2007-8-6-r116.
112. Blat Y, Protacio RU, Hunter N, Kleckner N. 2002. Physical and functional interactions among basic chromosome organizational features govern early steps of meiotic chiasma formation. Cell 111:791–802. https://doi.org/10.1016/S0092-8674(02)01167-4.
113. Raab JR, Kamakaka RT. 2010. Insulators and promoters: closer than we think. Nat Rev Genet 11:439–446. https://doi.org/10.1038/nrg2765.
114. Gehlen LR, Gruenert G, Jones MB, Rodley CD, Langowski J, O'Sullivan JM. 2012. Chromosome positioning and the clustering of functionally related loci in yeast is driven by chromosomal interactions. Nucleus 3:370–383. https://doi.org/10.4161/nucl.20971.
115. Baudat F, Nicolas A. 1997. Clustering of meiotic double-strand breaks on yeast chromosome III. Proc Natl Acad Sci U S A 94:5213–5218. https://doi.org/10.1073/pnas.94.10.5213.
116. Gerton JL, DeRisi J, Shroff R, Lichten M, Brown PO, Petes TD. 2000. Global mapping of meiotic recombination hotspots and coldspots in the yeast *Saccharomyces cerevisiae*. Proc Natl Acad Sci U S A 97:11383–11390. https://doi.org/10.1073/pnas.97.21.11383.
117. Bystricky K, Heun P, Gehlen L, Langowski J, Gasser SM. 2004. Long-range compaction and flexibility of interphase chromatin in budding yeast analyzed by high-resolution imaging techniques. Proc Natl Acad Sci U S A 101:16495–16500. https://doi.org/10.1073/pnas.0402766101.
118. Gartenberg MR, Neumann FR, Laroche T, Blaszczyk M, Gasser SM. 2004. Sir-mediated repression can occur independently of chromosomal and subnuclear contexts. Cell 119:955–967. https://doi.org/10.1016/j.cell.2004.11.008.
119. Taddei A, Gasser SM. 2004. Multiple pathways for telomere tethering: functional implications of subnuclear position for heterochromatin formation. Biochim Biophys Acta 1677:120–128. https://doi.org/10.1016/j.bbaexp.2003.11.014.
120. Schober H, Ferreira H, Kalck V, Gehlen LR, Gasser SM. 2009. Yeast telomerase and the SUN domain protein Mps3 anchor telomeres and

repress subtelomeric recombination. Genes Dev 23:928–938. https://doi.org/10.1101/gad.1787509.
121. Snider CE, Stephens AD, Kirkland JG, Hamdani O, Kamakaka RT, Bloom K. 2014. Dyskerin, tRNA genes, and condensin tether pericentric chromatin to the spindle axis in mitosis. J Cell Biol 207:189–199. https://doi.org/10.1083/jcb.201405028.
122. Casolari JM, Brown CR, Komili S, West J, Hieronymus H, Silver PA. 2004. Genome-wide localization of the nuclear transport machinery couples transcriptional status and nuclear organization. Cell 117:427–439. https://doi.org/10.1016/S0092-8674(04)00448-9.
123. Chen M, Gartenberg MR. 2014. Coordination of tRNA transcription with export at nuclear pore complexes in budding yeast. Genes Dev 28:959–970. https://doi.org/10.1101/gad.236729.113.
124. Gartenberg MR, Smith JS. 2016. The nuts and bolts of transcriptionally silent chromatin in *Saccharomyces cerevisiae*. Genetics 203:1563–1599. https://doi.org/10.1534/genetics.112.145243.
125. Fourel G, Lebrun E, Gilson E. 2002. Protosilencers as building blocks for heterochromatin. Bioessays 24:828–835. https://doi.org/10.1002/bies.10139.
126. Lebrun E, Revardel E, Boscheron C, Li R, Gilson E, Fourel G. 2001. Protosilencers in *Saccharomyces cerevisiae* subtelomeric regions. Genetics 158:167–176.
127. Gasser SM, Hediger F, Taddei A, Neumann FR, Gartenberg MR. 2004. The function of telomere clustering in yeast: the circe effect. Cold Spring Harbor Symp Quant Biol 69:327–337. https://doi.org/10.1101/sqb.2004.69.327.
128. Wang Y, Vujcic M, Kowalski D. 2001. DNA replication forks pause at silent origins near the HML locus in budding yeast. Mol Cell Biol 21:4938–4948. https://doi.org/10.1128/MCB.21.15.4938-4948.2001.
129. Lemoine FJ, Degtyareva NP, Lobachev K, Petes TD. 2005. Chromosomal translocations in yeast induced by low levels of DNA polymerase a model for chromosome fragile sites. Cell 120:587–598. https://doi.org/10.1016/j.cell.2004.12.039.
130. Admire A, Shanks L, Danzl N, Wang M, Weier U, Stevens W, Hunt E, Weinert T. 2006. Cycles of chromosome instability are associated with a fragile site and are increased by defects in DNA replication and checkpoint controls in yeast. Genes Dev 20:159–173. https://doi.org/10.1101/gad.1392506.
131. Kitada T, Schleker T, Sperling AS, Xie W, Gasser SM, Grunstein M. 2011. gammaH2A is a component of yeast heterochromatin required for telomere elongation. Cell Cycle 10:293–300. https://doi.org/10.4161/cc.10.2.14536.
132. Keogh MC, Kim JA, Downey M, Fillingham J, Chowdhury D, Harrison JC, Onishi M, Datta N, Galicia S, Emili A, Lieberman J, Shen X, Buratowski S, Haber JE, Durocher D, Greenblatt JF, Krogan NJ. 2006. A phosphatase complex that dephosphorylates gammaH2AX regulates DNA damage checkpoint recovery. Nature 439:497–501. https://doi.org/10.1038/nature04384.
133. Cole HA, Ocampo J, Iben JR, Chereji RV, Clark DJ. 2014. Heavy transcription of yeast genes correlates with differential loss of histone H2B relative to H4 and queued RNA polymerases. Nucleic Acids Res 42:12512–12522. https://doi.org/10.1093/nar/gku1013.
134. Ocampo J, Chereji RV, Eriksson PR, Clark DJ. 2016. The ISW1 and CHD1 ATP-dependent chromatin remodelers compete to set nucleosome spacing in vivo. Nucleic Acids Res 44:4625–4635. https://doi.org/10.1093/nar/gkw068.
135. Langmead B, Salzberg SL. 2012. Fast gapped-read alignment with Bowtie 2. Nat Methods 9:357–359. https://doi.org/10.1038/nmeth.1923.
136. Bray NL, Pimentel H, Melsted P, Pachter L. 2016. Near-optimal probabilistic RNA-seq quantification. Nat Biotechnol 34:525–527. https://doi.org/10.1038/nbt.3519.
137. Pimentel H, Bray NL, Puente S, Melsted P, Pachter L. 2017. Differential analysis of RNA-seq incorporating quantification uncertainty. Nat Methods 14:687–690. https://doi.org/10.1038/nmeth.4324.
138. Hediger F, Neumann FR, Van Houwe G, Dubrana K, Gasser SM. 2002. Live imaging of telomeres. yKu and Sir proteins define redundant telomere-anchoring pathways in yeast. Curr Biol 12:2076–2089. https://doi.org/10.1016/S0960-9822(02)01338-6.
139. Heun P, Laroche T, Shimada K, Furrer P, Gasser SM. 2001. Chromosome dynamics in the yeast interphase nucleus. Science 294:2181–2186. https://doi.org/10.1126/science.1065366.
140. Manning JE, Schmid CW, Davidson N. 1975. Interspersion of repetitive and nonrepetitive DNA sequences in the Drosophila melanogaster genome. Cell 4:141–155. https://doi.org/10.1016/0092-8674(75)90121-X.